Genome Biology

METHOD

Open Access

FixNCut: single-cell genomics through reversible tissue fixation and dissociation

Laura Jiménez-Gracia[1,2], Domenica Marchese[1,2], Juan C. Nieto[1,2], Ginevra Caratù[1,2], Elisa Melón-Ardanaz[3,4], Victoria Gudiño[3,4], Sara Roth[5,6,7], Kellie Wise[8,9,10], Natalie K. Ryan[9,11,12], Kirk B. Jensen[8,9,10], Xavier Hernando-Momblona[13,14], Joana P. Bernardes[15], Florian Tran[15,16], Laura Katharina Sievers[15,16], Stefan Schreiber[15,16], Maarten van den Berge[17,18], Tessa Kole[17,18], Petra L. van der Velde[18,19], Martijn C. Nawijn[18,19], Philip Rosenstiel[15], Eduard Batlle[13,14,20], Lisa M. Butler[9,11,12], Ian A. Parish[5,6], Jasmine Plummer[21], Ivo Gut[1,2], Azucena Salas[3,4], Holger Heyn[1,2,22*†] and Luciano G. Martelotto[8,9,22*†]

†Holger Heyn and Luciano G. Martelotto are joint senior authors.

*Correspondence: holger.heyn@cnag.eu; luciano.martelotto@adelaide.edu.au

[22] Omniscope, Barcelona, Spain
Full list of author information is available at the end of the article

Abstract

The use of single-cell technologies for clinical applications requires disconnecting sampling from downstream processing steps. Early sample preservation can further increase robustness and reproducibility by avoiding artifacts introduced during specimen handling. We present FixNCut, a methodology for the reversible fixation of tissue followed by dissociation that overcomes current limitations. We applied FixNCut to human and mouse tissues to demonstrate the preservation of RNA integrity, sequencing library complexity, and cellular composition, while diminishing stress-related artifacts. Besides single-cell RNA sequencing, FixNCut is compatible with multiple single-cell and spatial technologies, making it a versatile tool for robust and flexible study designs.

Keywords: Single-cell genomics, RNA sequencing, Sample fixation, Tissue dissociation, Cellular stress

Introduction

Single-cell sequencing has revolutionized our understanding of the complexity of life, allowing researchers to study tissues, organs, and organisms with unprecedented resolution [1]. However, most single-cell techniques are designed for freshly prepared specimens, which can present logistical challenges for decentralized study designs that require disconnecting the time and site of sampling from downstream processing steps. In this regard, preservation methods have been developed that enable sample collection and storage, expanding the applications of single-cell sequencing to personalized medicine and collaborative research. In addition to facilitating flexible study designs, early

sample preservation can improve robustness and reproducibility by reducing artifacts introduced during sample handling, such as differences in lab personnel skills, library preparation workflows, and sequencing technologies. Furthermore, preservation methods can mitigate cellular stress caused by external factors, such as sample collection, transport, storage, and downstream processing steps involving mechanical or enzymatic dissociation, which can alter transcriptomic profiles [2–4]. Such cellular stress can impact sample quality and confound downstream analyses by inducing early stress-response genes and altering the natural state of the cell. Therefore, early sample preservation can enhance the quality and reliability of single-cell sequencing studies, while enabling flexible and decentralized study designs.

Dissociation-induced artifacts can be mitigated by the use of cold-active proteases active at low temperatures (6 °C) to decrease transcriptional activity and the expression of heat shock and stress-response genes. However, digestion at low temperatures can result in changes in cell type abundance due to incomplete tissue dissociation [2]. Alternatively, inhibitors of transcription and translation have been shown to reduce gene expression artifacts by minimizing the impact of dissociation-induced stress [5]. To overcome the challenges associated with sample logistics in single-cell studies, cryopreservation has been established as a storage method that preserves transcriptional profiles of cells in suspension and solid tissues [4]. However, cryopreservation can result in reduced cell viability and induce considerable changes in sample composition, such as the depletion of epithelial cells, myeloid suppressor cells, and neutrophils [3, 6–8]. Alternatively, cells can be fixed using alcohol, such as ethanol or methanol, but this can cause structural damage due to dehydration, protein denaturation, and precipitation, potentially affecting transcriptomic profiles. Nevertheless, alcohol-based fixation has been shown to better maintain cell composition compared to cryopreservation in specific contexts [3, 9]. More recently, ACME (ACetic-MEthanol) fixation has been developed as a solution to simultaneously dissociate and fix tissues, resulting in high cellular and RNA integrity [10]. Although ACME has been demonstrated to be effective when combined with cryopreservation for cnidarian samples, its value for sample preparation across other species, including mouse and human, remains to be shown. Cross-linking fixatives, such as formaldehyde and paraformaldehyde (PFA), are used with specialized single-cell assays, but are incompatible with commonly applied high-throughput single-cell RNA sequencing (scRNA-seq) protocols measuring transcriptome by standard polyA-based expression capture (3′ end sequencing). Moreover, formaldehyde-based fixation generally impedes the application of single-cell multiome analysis, cellular indexing of transcriptomes, and epitopes sequencing (CITE-seq) [11, 12] or immune repertoire profiling, which relies on 5′ end sequencing. Finally, post hoc computational tools such as machine learning algorithms have been developed to reduce or remove dissociation-induced artifacts [13]. For a more comprehensive description of methods to mitigate dissociation-induced artifacts, we recommend referring to the review by Machado et al. [14]. However, due to the often larger biological compared to technical variability and the fact that not all cell types within a sample suffer the same stress, it is difficult to generalize bias correction across cells and samples [15].

To overcome the challenges discussed above, it was crucial to develop a standardized protocol for sample collection, cell stabilization, and tissue processing that allows for

fixation prior to sample processing. We present a workflow, called FixNCut, which uses Lomant's Reagent (dithiobis(succinimidyl propionate) (DSP)), a reverse crosslinker fixative, to enable tissue fixation prior to sample digestion steps. Such order of events prevents changes in gene expression during digestion and processing, while disconnecting sampling time and location from subsequent processing sites. DSP is a homo-bifunctional N-hydroxysuccinimide ester (NHS ester) crosslinker that contains an amine-reactive NHS ester at each end of an 8-carbon spacer arm. NHS esters react with primary amines at pH 7–9 to form stable amide bonds and release N-hydroxy-succinimide. Proteins typically have multiple primary amines in the side chain of lysine residues and the N-terminus of each polypeptide that can serve as targets for NHS ester crosslinking reagents. DSP is lipophilic and membrane-permeable, making it applicable for intracellular and intramembrane conjugation. However, it is insoluble in water and must be dissolved in an organic solvent before adding to the reaction mixture. The presence of a disulfide bond in the center of DSP makes its crosslinking reversible via reducing agents like DTT, which is present in most reverse transcription buffers of single-cell sequencing applications (e.g., 10x Genomics assays). To date, DSP has only been successfully used to preserve cells in suspension (cell culture or PBMCs) for single-cell sequencing in applications such as CLint-Seq, nanofluidic systems, or phosphoprotein-based cell selection [16–18], but it has not been employed in tissues prior to dissociation.

Here, we demonstrate the versatility of the FixNCut protocol to overcome key limitations in generating single-cell data across multiple tissues. We provide evidence that FixNCut preserves RNA integrity, library complexity, and cellular composition, while allowing for cell labeling or sample hashing prior to single-cell analysis. To illustrate its potential, we applied FixNCut to fix and digest mouse lung and colon tissue, as well as human colon biopsies from inflammatory bowel disease (IBD) patients, demonstrating its clinical utility. Additionally, we show that DSP fixation can be used in the context of spatial-omics, specifically multiplexing tissue imaging for spatial proteomics (i.e., Phenocycler).

Results

Reversible fixation of human cells in suspension

Extending previous studies using DSP to preserve cell lines for RNA sequencing [16], we initially confirmed its applicability for single-cell analysis of cells in suspension (human peripheral blood mononuclear cells; PBMCs) and microfluidics systems (10x Genomics Chromium Controller), before combining fixation and dissociation of complex solid tissues. To this end, we compared cell morphology, RNA integrity, and reverse transcription efficiency of fresh and DSP-fixed PBMCs. Fixed cells showed highly similar morphology compared to fresh PBMCs in bright-field microscopy, with no evident changes in cell phenotypes or sample clumping after fixation (Fig. S1a). Next, we captured and barcoded single cells from both fresh and DSP-fixed samples using the Next GEM Single Cell 3′ Reagent Kits v3.1 from 10x Genomics. Bioanalyzer profiles of the amplified cDNA from both samples were virtually identical, demonstrating DSP fixation not to affect RNA integrity or reverse transcription performance (Fig. S1b,c). After sequencing, we confidently mapped over 80% of the reads from both sequencing libraries to the human reference genome, with over 50% of exonic reads usable for quantifying

gene expression levels (Fig. 1a). We observed a comparable correlation between the number of detected genes or the number of unique molecular identifiers (UMIs) and sequencing depth for fresh and fixed samples (95% CI, 3.65e−05 ± 1.11e−05 and 0.44 ± 0.06 vs. 3.56e−05 ± 1.14e−05 and 0.35 ± 0.06, respectively), indicating DSP fixation to conserve library complexity (Fig. 1b). Briefly, we captured a total of 22,481 genes in both conditions, together with 1667 and 1482 specific for fresh and fixed samples, respectively. We confirmed this observation at the single-cell level, where we found a similar relationship between sequencing depth and the number of detected UMIs or genes per cell (Fig. S1d). In line, we observed similar gene counts in single blood cells in fresh and fixed samples (Fig. 1c). After filtering out low-quality cells, we found a similar distribution of the main quality control (QC) metrics between both protocols (Fig. S1e), except for a few specific cell subpopulations (Fig. S1f). These results suggest DSP fixation to conserve the ability to detect gene transcripts in single cells compared to fresh samples in scRNA-seq experiments.

To further assess potential technical variation between protocols, we identified highly variable genes (HVGs) independently in fixed and fresh PBMCs. We found that 70% of HVGs were shared between the two protocols, indicating a conserved representation of the transcriptome and suitability for joint downstream processing (Fig. S1g). Additionally, when we examined the variation captured in the main principal components (PCs) and displayed single-cell transcriptomes in two dimensions (uniform manifold approximation and projection; UMAP), we did not observe any notable outliers due to the sampling protocol (Fig. 1d). Cells clustered together based on biological differences rather than preparation protocol, suggesting fixed and fresh cells to have similar capacity for cellular phenotyping. The pseudo-bulk gene expression profiles between fixed and fresh samples were highly correlated ($R^2 = 0.99$, $p < 2.2e{-}16$) (Fig. 1e), indicating DSP fixation not to alter the expression of specific genes. This was further confirmed at the cell population level (Fig. S1h). Moreover, the biological processes such as apoptosis, hypoxia, reactive oxygen species (ROS), cell-cycle (G2/M checkpoint), unfolded protein response (UPR), and inflammation hallmarks remained unchanged across libraries (Fig. 1f).

Next, we performed a joint analysis of 17,483 fresh and fixed cells, which were clustered to define 19 distinct cell populations (Fig. 1g; Fig. S1i). All cell types and states were found across both protocols at similar proportions, except for classical monocytes and NK cells, which showed small but significant differences, being slightly increased in fresh and fixed, respectively (Fig. 1h). Fixation did not affect differential expression analysis (DEA), with only four upregulated genes representing hemoglobin subunits (*HBA1*, *HBA2*, and *HBB*) and a mitochondrial gene (*MT-NDL4*) (Fig. 1i; Additional file 2: Table 1). These genes were consistently found across all cell populations (Additional file 3: Table 2), a phenomenon also observed when performing digestion protocols at low temperatures [3]. The FixNCut protocol may prevent erythrocyte lysis, leading to their co-encapsulation with nucleated blood cells and the detection of specific transcripts.

Importantly, we observed a reduction in technical artifacts introduced during sample processing prior to single-cell experiments upon fixation. Specifically, gene expression alterations previously defined to correlate with ex vivo PBMC handling [19] showed a significant reduction upon fixation ($p < 2.2e{-}16$) (Fig. 1j). Moreover, a sampling-time gene signature obtained from single-cell benchmarking studies [4] also showed a

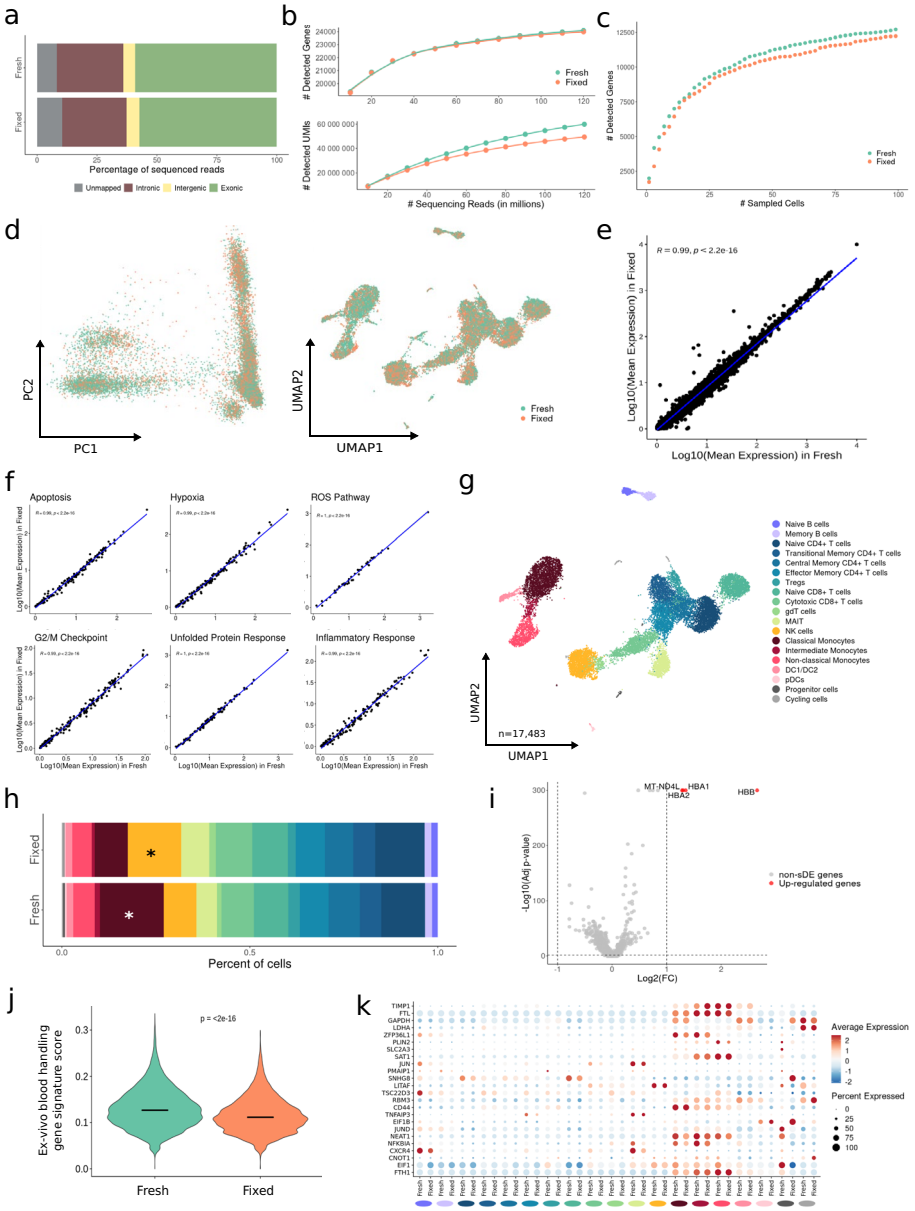

Fig. 1 FixNCut protocol in human peripheral blood mononuclear cells (PBMCs). **a** Mapping analysis of sequencing reads within a genomic region. **b** Comparative analysis of the number of detected genes (*top*) and UMIs (*bottom*) across various sequencing depths. **c** Cumulative gene counts analyzed using randomly sampled cells. **d** Principal component analysis (PCA) and uniform manifold approximation and projection (UMAP) representation of gene expression profile variances of fresh and fixed samples. **e**, **f** Linear regression model comparing average gene expression levels of expressed genes (**e**) and main biological hallmarks, including apoptosis, hypoxia, reactive oxygen species (ROS), cell cycle G2/M checkpoint, unfolded protein response (UPR), and inflammatory response genes (**f**). The coefficient of determination (R^2) computed with Pearson correlation and the corresponding *p*-value are indicated. **g** UMAP visualization of 17,483 fresh and fixed PBMCs, colored by 19 cell populations. **h** Comparison of cell population proportions between fresh (n = 9754) and fixed (n = 7729) PBMCs with the Bayesian model scCODA. Asterisks (*) indicate credible changes. **i** Differential gene expression analysis between fresh and fixed samples. The top differentially expressed genes (DEGs) with significant adjusted *p*-values (FDR) < 0.05, upregulated (red), and downregulated (blue) with Log2FC > |1| are indicated. **j** Violin plot of ex-vivo blood handling gene signature score [19] for fresh and fixed human PBMCs. Statistical analysis between fixed and fresh cells was performed using the Wilcoxon signed-rank test. **k** Dotplot showing the average expression of sampling-time DEGs for Fresh (*y*-axis) for all 19 cell types (*x*-axis) split by protocol. The dot size reflects the percentage of cells in a cluster expressing each gene, and the color represents the average expression level

significant reduction in the fixed PBMCs ($p < 2.2e{-}16$) (Fig. 1k). Interestingly, T lymphocytes appeared to be particularly affected ($p < 0.0001$; except for gdT cells, $p < 0.05$), showing the strongest protection from sampling artifacts in fixed cells (Fig. S1j). DSP also protected against the general reduction of gene expression activity, previously reported during PBMC sample processing [4]. Notably, more than 30% of genes from the sampling-time signature were also detected as enriched in the fresh PBMCs (Fig. S1k). The results suggest that fixed PBMCs have comparable cellular composition and gene expression profiles to freshly prepared samples, while reducing gene expression artifacts introduced during sample preparation.

FixNCut protocol applied on mouse solid tissues

Beyond the benefits of cell fixation in standardizing sample processing and preserving gene expression profiles of cells in suspension, the FixNCut protocol was specifically designed for solid tissues. Specifically, it allows for fixation and subsequent digestion, which is particularly advantageous for complex and logistically challenging study designs, such as clinical trials. Here, sampling artifacts, including biases in gene expression and cell type composition, are frequently observed in fragile solid tissue types. For example, differentiated colonic epithelial cells (e.g., secretory or absorptive cells), tightly connected adult neurons, or processing-sensitive adipocytes are more susceptible to cell damage and death as a result of common tissue dissociation protocols [20, 21]. Fixation prior to digestion using the FixNCut protocol can reduce these artifacts. Thus, we next evaluated the effectiveness of the FixNCut protocol with subsequent scRNA-seq readout in different solid mouse tissues before extending its application to challenging human patient samples, such as tissue biopsies.

Fresh mouse lung samples were minced, mixed, and split into two aliquots, one processed fresh and the other fixed using the FixNCut protocol with subsequent 30-min tissue digestion using Liberase TL. The fixed sample showed a slight decrease in cell size and an increase in DAPI+ cells, but overall, cell morphology was similar to the fresh sample (Fig. S2a). Single-cell encapsulation and scRNA-seq (10x Genomics, 3′ RNA v3.1) showed comparable proportions of reads mapped to the mouse reference genome and exonic genomic regions for both fresh and fixed samples (Fig. 2a). We further observed a similar correlation between the number of detected genes or UMIs and sequencing depth in fresh and fixed samples (95% CI, $2.31e{-}05 \pm 8.03e{-}06$ and 0.40 ± 0.06 vs. $2.64e{-}05 \pm 7.86e{-}06$ and 0.40 ± 0.06, respectively) (Fig. 2b). At the cell level, we confirmed the similar complexity of fixed libraries, as reflected by the number of detected UMIs and genes (Fig. S2b). Genes identified in both libraries ($n = 20{,}684$) were mostly protein-coding genes (76%). Conversely, genes exclusively captured in either fixed ($n = 1383$) or fresh ($n = 1157$) samples were largely non-coding RNA genes, specifically lncRNAs (52% vs 47%) (Fig. S2c). We further observed that more genes were captured for the fixed samples after accumulating information from a few number of individual lung cells (Fig. 2c). Importantly, after filtering out low-quality cells, the main QC metrics in fixed samples showed consistent distributions across all characterized cell types (Fig. S2d,e), suggesting that FixNCut protocol preserves the capacity for scRNA-seq profiling after fixation and digestion.

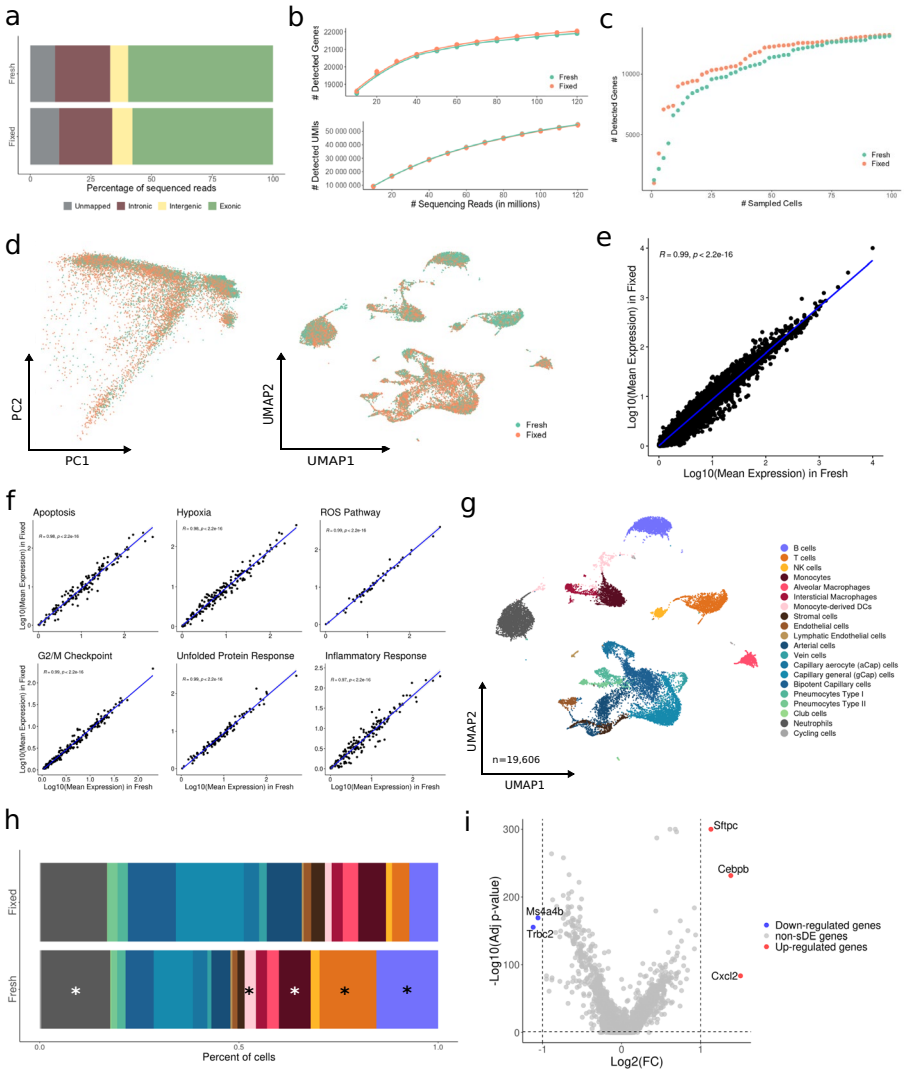

Fig. 2 FixNCut protocol tested in mouse lung samples. **a** Mapping analysis of sequencing reads within a genomic region. **b** Comparative analysis of the number of detected genes (*top*) and UMIs (*bottom*) across various sequencing depths. **c** Cumulative gene counts analyzed using randomly sampled cells. **d** Principal component analysis (PCA) and uniform manifold approximation and projection (UMAP) representation of gene expression profile variances of fresh and fixed samples. **e** Linear regression model comparing average gene expression levels of expressed genes between protocols. The coefficient of determination (R^2) computed with Pearson correlation is indicated. **f** Hierarchical clustering of coefficient of determination (R^2) obtained for all pair comparisons between protocols for biological hallmarks, including apoptosis, hypoxia, reactive oxygen species (ROS), cell cycle G2/M checkpoint, unfolded protein response (UPR), and inflammatory response genes. **g** UMAP visualization of 19,606 fresh and fixed mouse lung cells, colored by 20 cell populations. **h** Comparison of cell population proportions between fresh (n = 10,289) and fixed cells (n = 9317). The top figure shows the difference in cell population proportions between fresh and fixed samples, and the bottom figure shows the results of the compositional cell analysis using the Bayesian model scCODA. Asterisks (*) indicate credible changes, upregulated for the fresh sample. **i** Differential gene expression analysis between fresh and fixed samples. The top differentially expressed genes (DEGs) with significant adjusted p-values (FDR) < 0.05, upregulated (red), and downregulated (blue) with Log2FC > |1| are indicated

An overlap of almost 80% of sample-specific HVGs was found when comparing the fresh and FixNCut protocols (Fig. S2f). The absence of batch effects linked to protocols was demonstrated by the PCA and UMAP representations (Fig. 2d), indicating bias-free transcriptome profiles after cell fixation and digestion. Highly comparable

profiles of mean gene expression values were observed between fresh and fixed mouse lung samples ($R^2 > 0.99$, $p < 2.2e{-}16$) (Fig. 2e), a finding also confirmed at the population level (Fig. S2g). Moreover, the high correlation across gene programs supported the absence of alterations in major biological processes (Fig. 2f).

We then performed a joint analysis of all 19,606 mouse lung cells, which were segregated into 20 distinct cell populations, encompassing both lung and tissue-resident immune cells (Fig. 2g; Fig. S2h). All characterized cell types were detected in both fresh and fixed samples, with slight variability in cell type proportions between both protocols. The fixed protocol showed an improved representation of tightly connected epithelial and endothelial cell types, while immune cells (B and T cells, monocytes, monocyte-derived DCs, and neutrophils) were proportionally increased in the fresh sample (Fig. 2h). To validate preserved gene expression profiles in fixed tissues, we performed differential expression analysis (DEA) between the two protocols. We observed upregulation of genes related to pneumocytes (*Sftpc*), myeloid enhancer binding protein (*Cebpb*), and endothelial cells promoting cell migration (*Cxcl2*) for the fixed protocol, which could be largely explained by the enrichment of this population upon fixation. In contrast, fresh samples were enriched in genes related to inflammatory and immune processes (*Ms4a4b* and *Trbc2*), in accordance with the increased proportion of recovered immune cells (Fig. 2i; Additional file 4: Table 3). At the cellular level, we found a uniform enrichment in stress-related genes in non-immune populations from the fresh sample, while the fixed sample showed this enrichment in immune populations (Additional file 5: Table 4). Gene set enrichment analysis (GSEA) stratified by cell type revealed that freshly prepared endothelial cells were enriched in ROS, apoptosis, and cellular response to external stimuli, whereas the opposite patterns were observed upon fixation (Additional file 6: Table 5). Overall, these results suggest the global conservation of library complexity and quality, along with the inclusion of tightly connected, challenging-to-isolate cell types in fixed mouse lung samples.

We further evaluated the performance of the FixNCut protocol in a different challenging solid tissue context. To do so, we minced and mixed mouse colon samples that were split and subjected to scRNA-seq after digestion of either fresh or fixed tissues. Our results indicate that FixNCut provides several benefits, including improved transcriptome capture accuracy, as evidenced by a higher number of total reads mapped to the reference and a higher exonic fraction (Fig. 3a). Additionally, the fixed sample exhibited a higher non-significant library complexity based on the total number of detected genes (95% CI, 8.81e−05 ± 2.83e−05 vs. 9.03e−05 ± 3.16e−05) coupled with an increased number of total UMIs at deeper sequencing (95% CI, 0.71 ± 0.05 vs. 0.73 ± 0.07) (Fig. 3b), with fixed cells showing increased numbers of detected UMIs and genes (Fig. S3a). Genes identified in both libraries ($n = 18{,}314$) were mostly protein-coding genes (81%). Conversely, genes exclusively captured in fixed samples ($n = 2225$) compared to those from fresh ($n = 1011$) showed a larger percentage of protein-coding (45% vs 35%) coupled with a smaller fraction of lncRNA (44% vs 53%) (Fig. S3b), indicating that FixNCut enhances the gene capture efficiency, potentially allowing for a more fine-grained cell phenotyping after sample fixation. Notably, the

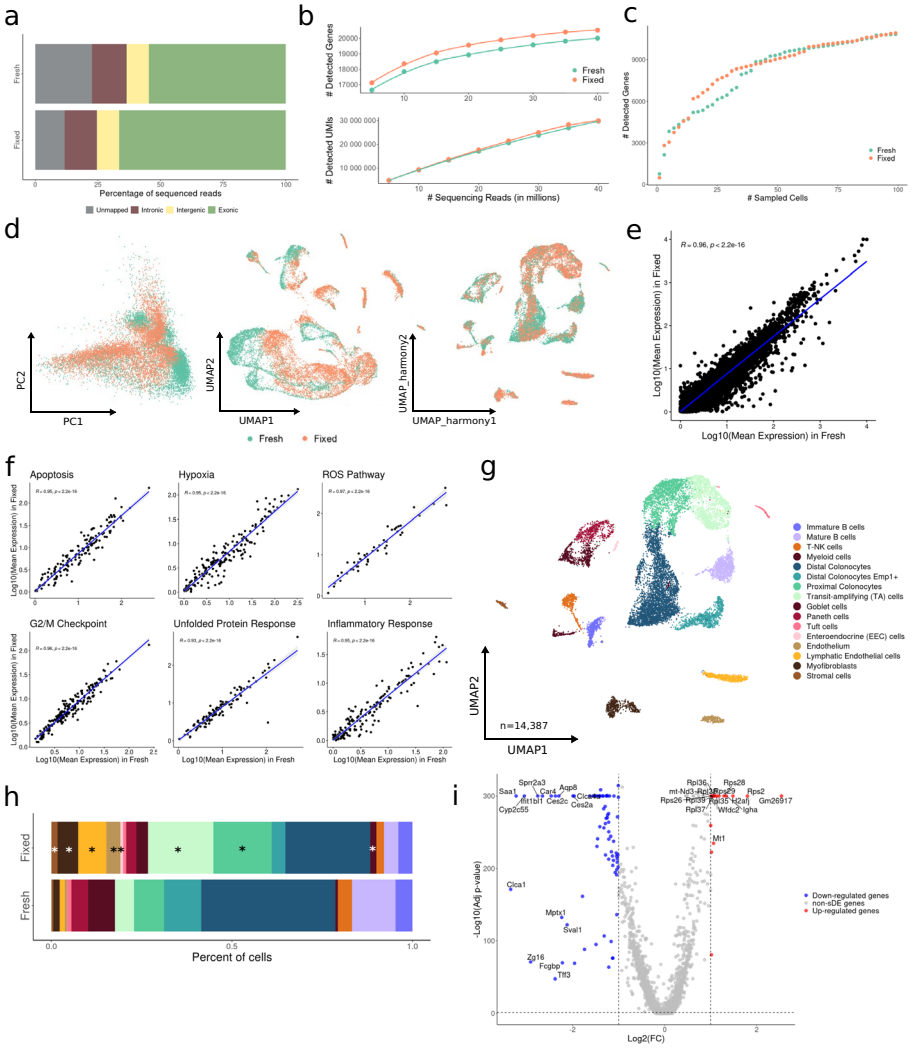

Fig. 3 FixNCut protocol tested in mouse colon samples. **a** Mapping analysis of sequencing reads within a genomic region. **b** Comparative analysis of the number of detected genes (*top*) and UMIs (*bottom*) across various sequencing depths. **c** Cumulative gene counts analyzed using randomly sampled cells. **d** Principal component analysis (PCA), uniform manifold approximation and Projection (UMAP) prior data integration, and *harmony* integrated UMAP representation of gene expression profile variances of fresh and fixed samples. **e**, **f** Linear regression model comparing average gene expression levels of expressed genes (**e**) and biological hallmarks, including apoptosis, hypoxia, reactive oxygen species (ROS), cell cycle G2/M checkpoint, unfolded protein response (UPR), and inflammatory response genes (**f**). The coefficient of determination (R^2) computed with Pearson correlation and the corresponding p-values are indicated. **g** UMAP visualization of 14,387 fresh and fixed mouse colon cells, colored by 16 cell populations. **h** Comparison of cell population proportions between fresh ($n = 6009$) and fixed ($n = 8378$) mouse colon samples with the Bayesian model scCODA. Asterisks (*) indicate credible changes, upregulated for the fixed sample. **i** Differential gene expression analysis between fresh and fixed samples. The top differentially expressed genes (DEGs) with significant adjusted *p*-values (FDR) < 0.05, upregulated (red), and downregulated (blue) with Log2FC > |1| are indicated

cumulative gene count was greater for the fixed colon, particularly when considering a larger number of sampled cells (Fig. 3c), and we observed improved QC metrics for the FixNCut sample after filtering out low-quality cells, which held true across all cell populations (Fig. S3c,d).

The overlap of HVGs between the fresh and fixed colon samples was slightly lower than that observed in lung tissues (> 60%) (Fig. S3e). Further, we identified noticeable differences in the transcriptomic profile, as demonstrated in both PCA and UMAP representations (Fig. 3d), which were attributed to the aforementioned improvements in library complexity after DSP fixation. Given that the overall cellular transcriptomic profile remains intact, confirmed by a high correlation in mean gene expression values between the two protocols ($R^2 = 0.96$, $p < 2.2e{-}16$) (Fig. 3e, f), we applied sample integration to collectively annotate cells and to address technical differences at cell type level (Fig. 3d). Notably, cell populations that exhibited a diminished correlation between the fresh and fixed samples coincided with cell types that were specifically enriched in the fixed sample (Fig. S3f).

We captured a total of 14,387 cells that were clustered into 16 cell populations, representing both immune and colon-epithelium cells (Fig. 3g; Fig. S3g). All cell types were detected in both conditions, but we observed a clear shift in cell type composition with an enrichment of sensitive epithelial and stromal cells in the fixed sample (Fig. 3h). Differential expression analysis revealed a higher representation of ribosomal protein and mitochondrial genes in the fixed sample, mostly explained by the larger capture of actively cycling epithelial cell population known as transit-amplifying (TA) cells (Fig. 3i; Additional file 4: Table 3). In line, both epithelial and stromal populations were also enriched in mitochondrial and ribosomal protein genes (Additional file 7: Table 6). Additionally, GSEA by cell population showed enrichment of ribosomal-dependent and metabolic processes pathways in fixed cells, especially in the sensitive populations (Additional file 8: Table 7). Together, our results demonstrate the FixNCut protocol to enhance library complexity and quality metrics, while also capturing fragile epithelial and stromal cell populations from delicate tissues, such as the colon. Thus, DSP-based fixation preserves the integrity of tightly connected cell types that are otherwise difficult to isolate for single-cell experiments, resulting in an improved representation of cell types and states in these solid tissues.

Long-term storage of fixed tissues

Conducting multi-center clinical studies can be challenging due to centralized data production and the need for storage and shipment. To address this challenge, we evaluated the combination of the FixNCut protocol with cryopreservation (cryo; 90% FBS and 10% DMSO; see the "Methods" section) to allow for the separation of sampling time and location from downstream data generation, while preserving sample composition and gene expression profiles. To test this, fresh mouse lung samples were minced, mixed, and split into three pools for fixation-only, cryo-only, and fixation+cryo sample processing. After single-cell capture and sequencing (10x Genomics, 3′ RNA v3.1), all three libraries showed comparable statistics of mapped and exonic reads across conditions, indicating successful preservation of the transcriptome (Fig. 4a). We also observed a similar relationship between the number of detected genes and the sequencing depth for all three protocols (95% CI, 2.88e−05 ± 8.64e−06 cryo vs. 2.37e−05 ± 8.07e−06 fixed/cryo), although the number of detected UMIs was statistically significantly reduced in the fixed/cryo sample compared to cryo-only (95% CI, 0.46 ± 0.06 cryo vs. 0.24 ± 0.06 fixed/cryo) (Fig. 4b), which was consistent considering the detected UMIs and genes

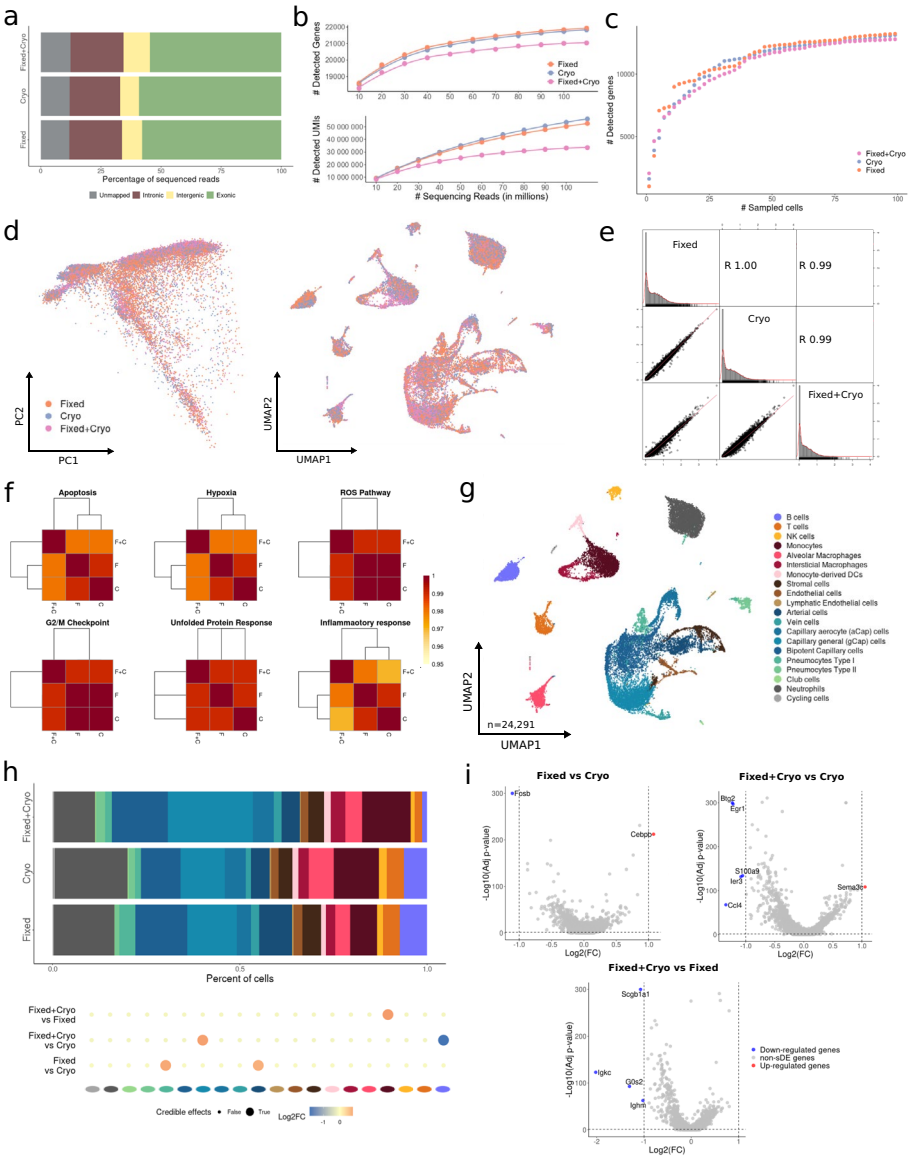

Fig. 4 Long-term storage of fixed mouse lung samples. **a** Mapping analysis of sequencing reads within a genomic region. **b** Comparative analysis of the number of detected genes (*top*) and UMIs (*bottom*) across various sequencing depths. **c** Cumulative gene counts analyzed using randomly sampled cells. **d** Principal component analysis (PCA) and uniform manifold approximation and projection (UMAP) representation of gene expression profile variances of fixed, cryopreserved, and fixed/cryopreserved samples. **e** Linear regression model comparing average gene expression levels of expressed genes across protocols used. The coefficient of determination (R^2) computed with Pearson correlation is indicated. **f** Hierarchical clustering of coefficient of determination (R^2) obtained for all pair comparisons across protocol for biological hallmarks, including apoptosis, hypoxia, reactive oxygen species (ROS), cell cycle G2/M checkpoint, unfolded protein response (UPR), and inflammatory response genes. **g** UMAP visualization of 24,291 fixed, cryo, and fixed/cryo mouse lung cells, colored by 20 cell populations. **h** Comparison of cell population proportions between fixed (n = 10,256), cryopreserved (n = 8609), and fixed/cryopreserved cells (n = 5426). The top figure shows the difference in cell population proportions between fixed, cryo, and fixed/cryo samples, and the bottom figure shows the results of the compositional cell analysis using the Bayesian model scCODA. Credible changes and Log2FC are indicated. **i** Differential gene expression analysis across conditions: fixed vs cryo (*top-left*), fixed/cryo vs cryo (*top-right*), and fixed/cryo vs fixed (*bottom*). The top differentially expressed genes (DEGs) with significantly adjusted *p*-values (FDR) < 0.05, upregulated (red), and downregulated (blue) with Log2FC > |1| are indicated

across individual cells (Fig. S4a), but hardly noticeable when accumulating gene counts across multiple cells (Fig. 4c). Genes identified across all libraries (n = 19,509) were mostly protein-coding genes (78%). Conversely, genes exclusively captured in fixed/cryo samples compared to those from cryo-only showed a similar percentage of protein-coding genes (34% vs 36%) and comparable fractions of lncRNA (52% vs 50%) (Fig. S4b). After removing low-quality cells, we found highly comparable distributions for the main QC metrics across all samples. However, we noticed a small increase in the percentage of mitochondrial gene expression detected in the fixed/cryo sample (Fig. S4c). Similarly, the different cell populations showed consistent QC across conditions (Fig. S4d).

We confirmed the absence of DSP-fixation biases after cryopreserving fixed samples, as indicated by a high overlap (> 70%) of HVGs across all three protocols (Fig. S4e). In addition, both PCA and UMAP dimensionality reduction plots showed no discernible biases between preservation protocols (Fig. 4d). We also observed highly comparable expression profiles and gene programs when correlating the mean gene expression values for all protocol comparisons ($R^2 > 0.99$, $p < 2.2e{-}16$) (Fig. 4e). Moreover, there was no appreciable alteration in biological processes at the gene program or population level when comparing across protocols (Fig. 4f; Fig. S4f).

We next analyzed 24,291 mouse lung cells processed with the three different protocols and annotated 20 lung and tissue-resident immune cell populations (Fig. 4g; Fig. S4g), and all cell types and states were found across the three conditions at similar proportions. However, we observed slight changes in composition, with fixed/cryo samples showing a decrease of B cells coupled with an increase of gCap compared to the cryo sample, and an increase of Monocytes compared to fixed-only. Comparing fixed-only with cryo, we found an increase in arterial and pneumocyte type I cells compared to the cryo sample (Fig. 4h). Additionally, we observed downregulation of genes associated with immune function (e.g., *Igkc*, *Ccl4*, *Scgb1a1*) in the fixed/cryo, explained by the aforementioned shift in cell type composition. Importantly, the cryo-only sample showed upregulated genes related to stress response, such as *Fosb* (Fig. 4i; Additional file 4: Table 3). A closer inspection of the different cell populations validated the expression of stress-related genes across all cells in the cryo-only compared fixed/cryo samples, specifically in non-immune cells (Additional file 9: Table 8). Accordingly, GSEA detected an enrichment of regulatory or response pathways for almost all cryopreserved cell types compared to fixed/cryo samples (Additional file 10: Table 9). These results support the feasibility of cryopreservation after fixation to combine the robustness and logistical advantages of the respective methods for scRNA-seq experiments.

Minimization of technical artifacts in FixNCut tissue samples

Fixing tissues after sample collection preserves the natural state of a cell and avoids technical biases, previously shown to affect bulk and single-cell transcriptomics analysis [2–4, 22]. In addition to the abovementioned differences in stress-response genes, we further aimed to demonstrate the ability of FixNCut to preserve gene expression profiles by examining previously identified artifact signatures. Specifically, we investigated condition-specific gene signatures from published studies using our mouse lung and colon data (see the "Methods" section).

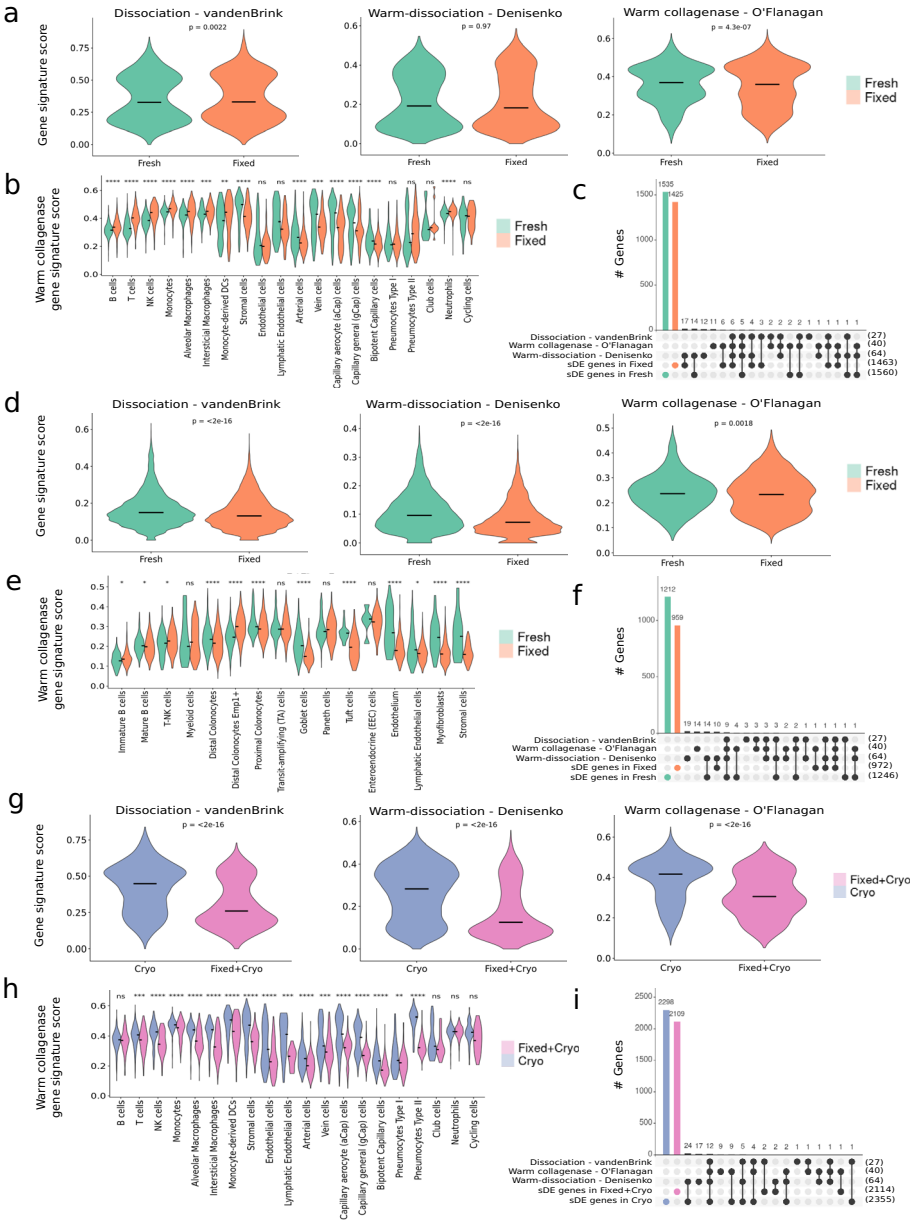

Fig. 5 Minimization of technical artifacts using FixNCut protocol on mouse tissues. This figure shows the impact of various dissociation-induced gene signature scores, including dissociation on mouse muscle stem cells [22], warm dissociation on mouse kidney samples [3], and warm collagenase dissociation on mouse primary tumors and patient-derived mouse xenografts [2], across mouse tissues and processing protocols used. All statistical analyses between protocols were performed using the Wilcoxon signed-rank test; significance results are indicated with the adjusted *p*-value, either with real value or approximate result (ns, $p > 0.05$, *$p \leq 0.05$, **$p \leq 0.01$, ***$p \leq 0.001$, ****$p \leq 0.0001$). **a** Violin plots of dissociation-induced gene signatures scores for fresh and fixed mouse lung. **b** Score of warm collagenase gene signature for fresh and fixed mouse lung samples across cell populations. **c** Overlap of differentially expressed genes in the fresh and fixed mouse lung sample with genes from the three dissociation-induced signatures. **d** Violin plots of dissociation-induced gene signatures scores for fresh and fixed mouse colon. **e** Score of warm collagenase gene signature for fresh and fixed mouse colon samples across cell populations. **f** Overlap of differentially expressed genes in the fresh and fixed mouse colon sample with genes from the three dissociation-induced signatures. **g** Violin plots of dissociation-induced gene signatures scores for cryo and fixed/cryo mouse lung. **h** Score of warm collagenase gene signature for cryo and fixed/cryo mouse lung samples across cell populations. **i** Overlap of differentially expressed genes in the cryopreserved and Fixed/Cryo mouse lung sample with genes from the three dissociation-induced signatures

After analyzing mouse lung samples, we found that fixed samples had comparable dissociation/temperature-signature scores, except for the warm collagenase which was significantly lower ($p < 4.3e{-}07$) compared to fresh samples (Fig. 5a). We observed that external tissue stressors had a greater impact on fresh lung resident cells compared to the infiltrating immune cell fraction (Fig. 5b). Interestingly, the signature scores for these populations displayed a bimodal-like distribution, indicating an uneven effect within cell populations (Fig. 5b). Additionally, stress-signature genes were not only found to be differentially expressed in the fresh lung but also in the fixed samples, regardless of their level of expression (Fig. 5c).

Similarly, fixed colon samples showed a significantly larger decrease in dissociation/temperature-stress signature scores compared to fresh samples (Fig. 5d). Here, we also observed a lineage-dependent impact of cell stress; colonocytes were greatly affected with differences in subtypes, whereas immune cells largely escaped stress biases (Fig. 5e). Endothelial and stromal cells suffered the largest dissociation-related stress in the fresh samples, which was drastically reduced upon fixation (Fig. 5e). Moreover, stress-signatures genes were also differentially expressed in the fresh colon sample, while largely absent in the fixed sample (Fig. 5f).

Furthermore, we demonstrated the effectiveness of FixNCut for long-term sample storage by examining the dissociation/temperature-stress signature scores in cryo-only and fixed/cryo mouse lung samples. Our results showed that cryopreserved samples had significantly higher stress-related signature scores compared to fixed/cryo ($p < 2.2e{-}16$) (Fig. 5g). Interestingly, the stress signature score for endothelial and stromal cells exhibited a bimodal distribution exclusively in the cryo-only sample, with cells showing larger dissociation-related effects in the same population (Fig. 5h), consistent with previous observations. Over 70% of signature-specific genes were significantly differentially expressed in the cryo-only sample, an even higher proportion compared to fresh lung and colon samples, whereas the fixed/cryo samples had almost no overlapping DEGs (Fig. 5i).

Moving towards the use of FixNCut on clinical samples

As a proof-of-concept for a multi-center clinical research study focused on autoimmune diseases, we evaluated the performance of FixNCut on human patient biopsies. To this end, we obtained fresh colon biopsies from two IBD patients in remission. The biopsies were mixed and split into four aliquots, which were processed as follows: fresh, fixed-only, cryo-only, or fixed/cryo. The fixed human colon samples exhibited a similar proportion of reads mapped to the reference genome and exonic regions as mouse colon tissues (Fig. 6a) and displayed comparable library complexity for short-term (fixed vs. fresh) and long-term (fixed/cryo vs. cryo) conditions, considering the total number of detected genes (95% CI $6.29e{-}05 \pm 2.03e{-}05$ fresh vs. $5.53e{-}05 \pm 2.13e{-}05$ fixed; $6.65e{-}05 \pm 2.23e{-}06$ cryo vs. $6.10e{-}05 \pm 2.11e{-}05$ fixed/cryo) and captured UMIs (95% CI 0.48 ± 0.07 fresh vs. 0.37 ± 0.08 fixed; 0.47 ± 0.07 cryo vs. 0.39 ± 0.08 fixed/cryo) (Fig. 6b). A similar pattern was observed comparing the number of captured genes and UMIs at the cell level (Fig. S5a). The cumulative detected gene count was highest for the fixed biopsy, with fresh being the worst condition (Fig. 6c). Genes identified across all libraries ($n = 21{,}637$) were mostly protein-coding genes (70%), followed by

non-annotated genes (21%). Genes exclusively captured in one condition (fresh, fixed, cryo-only, or fixed/cryo) showed a highly similar distribution of gene features (Fig. S5b). After removing low-quality cells, the main quality control metrics had similar distributions, with slightly improved median UMI, gene counts, and reduced mitochondrial gene percentage for the fixed sample (Fig. S5c), which were consistently observed across almost all populations (Fig. S5d). We observed an overlap (> 50%) of HVGs across all conditions (Fig. S5e) and although subtle protocol-associated effects were found, we ensure a consistent cell annotation across samples after successful sample integration (Fig. 6d). Gene expression profiles and gene programs significantly correlated across all samples ($R^2 > 0.96$, $p < 2.2e{-}16$) (Fig. 6e, f), with a slightly reduced correlation observed in M0 macrophages and stromal cells (Fig. S5f).

By jointly analyzing 17,825 IBD colon cells across protocols, we identified 21 major cell types, including both colon and tissue-resident as well as infiltrated immune cells (Fig. 6g; Fig. S5g). All cell types and states were found across all protocols at similar proportions, although the number of high-quality cells was reduced in the cryo-only sample (Fig. 6h). Notably, the FixNCut protocol captured larger proportions of CD4+ T and B cells compared to fresh or cryo-only samples, among other minor changes (Fig. 6h). We also found that fixed samples had downregulation of heat-shock proteins (HSP), such as *HSPA1A*, *HSPA1B*, and *DNAJB1*, and upregulation of B cell-specific genes, including *MS4A1*, *HLA-DRA*, *HLA-B*, and *CXCR4*, when compared to fresh and cryo-only human colon samples (Fig. 6i; Additional file 11: Table 10). In line with the findings from the mouse experiment, we observed that fixed human colon samples exhibited increased expression of ribosomal genes (related to TA cells) at the cell population level, whereas fresh samples showed higher mitochondrial expression. Apart from increased HSP genes in the cryo-only sample, no other significant differentially expressed genes were found between the conditions (Additional file 12: Table 11; Additional file 13: Table 12). GSEA revealed the cryo-only sample to be enriched in stress pathways (response to external stimuli such as stress, temperature,

(See figure on next page.)

Fig. 6 FixNCut protocol tested in human colon biopsies. **a** Mapping analysis of sequencing reads within a genomic region. **b** Comparative analysis of the number of detected genes (*top*) and UMIs (*bottom*) across various sequencing depths. **c** Cumulative gene counts analyzed using randomly sampled cells. **d** Principal component analysis (PCA) and uniform manifold approximation and projection (UMAP) representation of gene expression profile variances prior data integration, and *harmony* integrated UMAP representation of gene expression profile variances of fresh, fixed, cryopreserved, and fixed/cryopreserved samples. **e** Linear regression model comparing average gene expression levels of expressed genes across protocols used. The coefficient of determination (R^2) computed with Pearson correlation is indicated. **f** Hierarchical clustering of coefficient of determination (R^2) obtained for all pair comparisons across protocols for biological hallmarks, including apoptosis, hypoxia, reactive oxygen species (ROS), cell cycle G2/M checkpoint, unfolded protein response (UPR), and inflammatory response genes. **g** UMAP visualization of 17,825 fresh, fixed, cryopreserved, and fixed/cryopreserved human colon cells, colored by 21 cell populations. **h** Comparison of cell population proportions between fresh ($n = 5759$), fixed ($n = 4250$), cryo ($n = 3489$), and fixed/cryo ($n = 4327$) cells. The bottom figure shows the results of compositional cell analysis using the Bayesian model scCODA. Credible changes and Log2FC are indicated. **i** Differential gene expression analysis across conditions: fixed vs fresh (*top-left*), fixed vs cryo (*top-right*), fixed/cryo vs cryo (*bottom-left*), and fixed/cryo vs fixed (*bottom-right*). Significant adjusted *p*-values (FDR) < 0.05, upregulated (red), and downregulated (blue) genes with Log2FC > |1| are indicated. The top DE genes are included in the plot. **j** Violin plots for stress-related gene signature score [2, 3, 22] for human colon biopsies across protocols. Statistical analysis between protocols was performed using the Wilcoxon signed-rank test

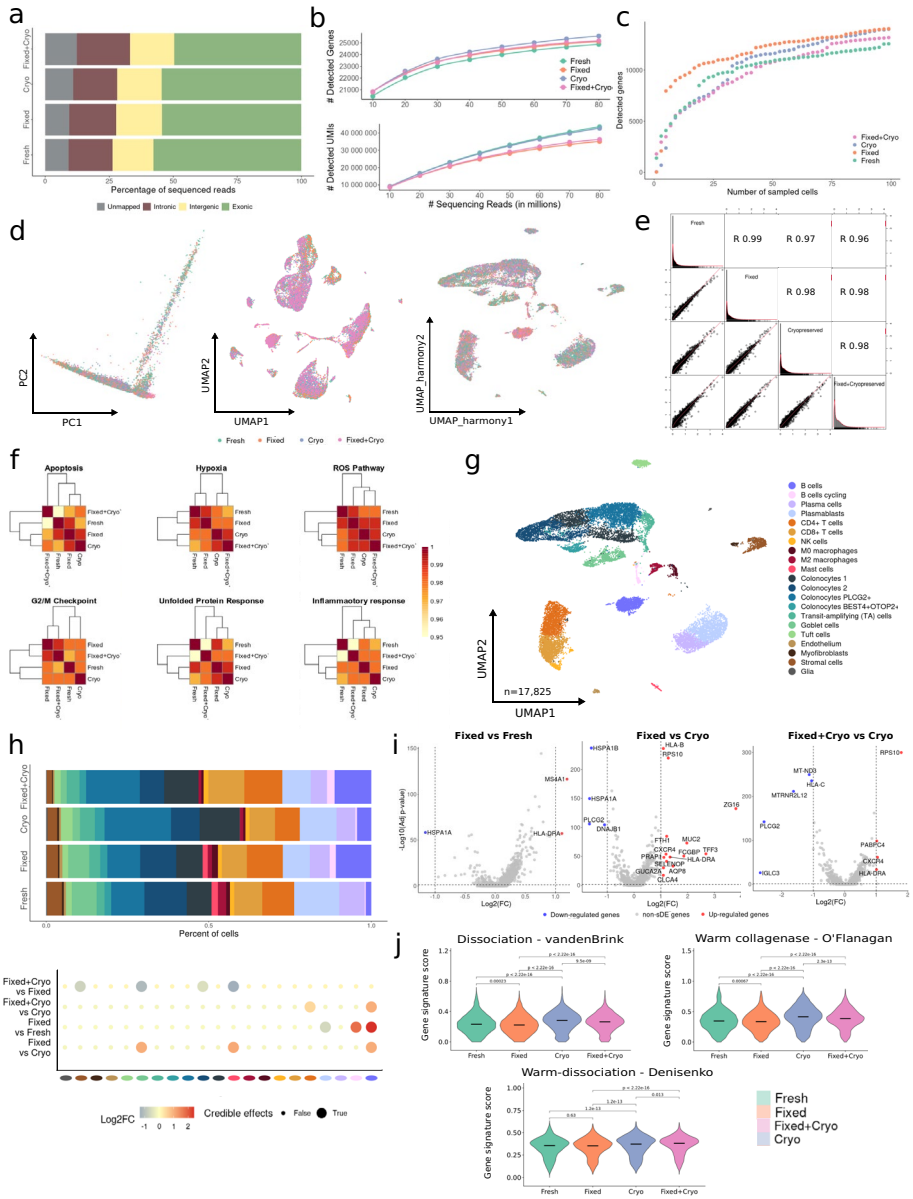

Fig. 6 (See legend on previous page.)

oxidative stress, and protein folding), a pattern also observed in the fixed/cryo sample compared to fixed, but restricted to immune cell types (Additional file 14: Table 13; Additional file 15: Table 14).

By comparing published stress signatures (see the "Methods" section) across fresh, fixed-only, cryo-only, and fixed/cryo samples, we found no significant differences between the fixed and fresh samples, whereas the cryo-only sample had significantly higher scores than the fresh sample, with the fixed/cryo sample presenting a lower stress scores than the cryo-only sample, indicating a reduction of gene expression artifacts by fixation for long-term storage in patient biopsies (Fig. 6j). We observed no significant cell population-specific effect; however, stromal cells had the highest score compared to other (Fig. S5h). These findings provide proof-of-concept evidence for the applicability

and value of FixNCut in improving the robustness of data generation in the clinical setting.

Expanding the application of FixNCut to various single-cell techniques

Next, we assessed the compatibility of the FixNCut protocol with single-cell application variants that involve cell labeling with antibodies or lipids targeting the cell membrane (e.g., FACS, CITE-seq, cell hashing). To this end, we stained fresh, cryopreserved, and fixed PBMCs and colon tissue samples with fluorescent antibodies or lipid-modified oligos (LMOs), which were analyzed by flow cytometry.

First, we analyzed a cohort of cryopreserved and cryo+fixed human PBMCs ($n = 3$) stained with anti-CD3, CD4, CD8, and CD19 monoclonal antibodies (mAbs). The analysis of cell morphology and viability showed that DSP fixation induced slight changes in cell size, internal complexity, and membrane permeability of PBMCs. Specifically, lymphocytes showed a decrease in forward scatter (cell size), while monocytes showed a decrease in side scatter (internal complexity) (Fig. S6a,b). Next, cells were gated based on the expression of CD3, CD4, and CD8 to characterize all T cell subtypes, and CD19 for B cells. We confirmed that DSP fixation did not alter the percentage of any of the immune cell types analyzed (Fig. 7a). However, using the same amount of antibodies, the mean fluorescence intensity (MFI) was higher in the cryopreserved compared to the cryo+fixed PBMCs (Fig. 7b). To ensure cryopreservation did not introduce any bias, we analyzed another cohort of fresh and fixed human PBMCs ($n = 4$) stained with anti-CD45, CD3, CD4, and CD8 mAbs and against ubiquitously expressed human surface proteins (β2M and CD298) and LMOs for cell hashing and multiplexing. DSP fixation led to an increased binding of DAPI, Annexin V (apoptotic cell marker), and propidium iodine (necrotic cell marker) in PBMCs, indicating reduced membrane integrity, particularly after storing cells at 4 °C for 2 days (Fig. S6c). These changes in morphology and membrane integrity should be taken into account when working with mixed study designs including both fixed and fresh samples. Despite observing a minor decrease in the MFI for most of the tested antibodies in fixed samples, we did not detect significant differences in cell type composition comparing fresh to fixed cells (Fig. 7c; Fig. S6d). Similarly, whereas PBMCs labeled with β2M and CD298 antibodies showed no differences in MFI between protocols, cells stained with LMOs revealed a minor but noticeable reduction in signal strength in fixed cells (Fig. 7d).

Similarly, staining dissociated human colon biopsies with anti-CD45, CD3, CD11b, and EpCAM antibodies showed similar MFI in cryopreserved and fixed cells (Fig. 7f; Fig. S6e). Our results showed that DSP fixation is compatible with cell labeling of cells with antibodies. Nevertheless, we recommend the optimization of labeling conditions and flow cytometry protocol of fixed samples, depending on antibody sensitivity, antigen abundance, and downstream applications, to further improve results.

Finally, we explored the potential applicability of DSP-fixed tissues in spatial technologies. We applied DSP-fixed tissue to spatial proteomics using multiplexed immunofluorescence tissue imaging, formerly known as co-detection by indexing (CODEX) [23]. We analyzed a DSP-fixed paraffin-embedded prostate cancer sample and its formalin-fixed counterpart using the commercial Phenocycler instrument (Akoya Biosciences). DSP-fixed sections exhibited a pattern of expression and signal intensity comparable

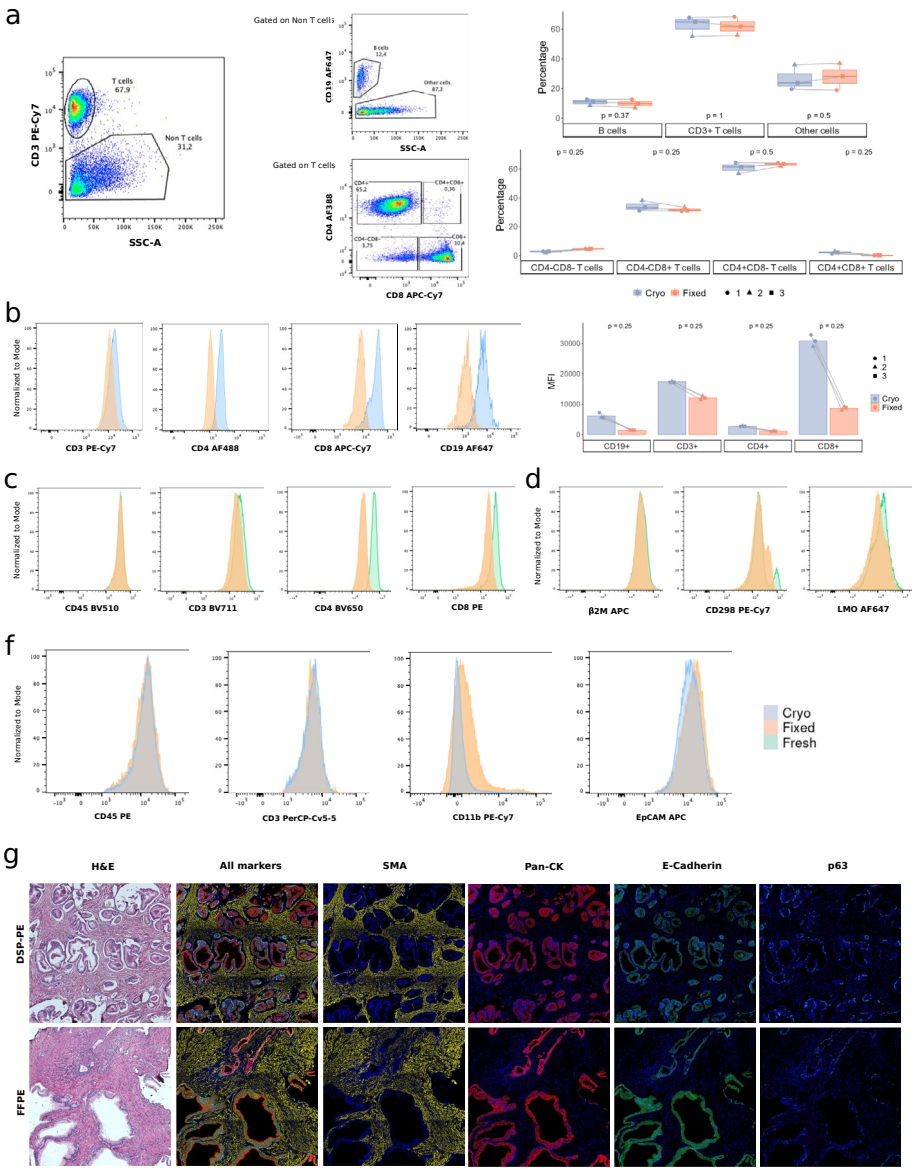

Fig. 7 Fluorescent antibody labeling of membrane proteins in fixed cells and tissues in mouse and human. **a** Representative gating strategy of one experiment analyzed by flow cytometry with cryopreserved and cryopreserved+fixed PBMCs from healthy donors ($n = 3$). PBMCs were stained with anti-human CD45, CD3, CD19, CD4, and CD8 monoclonal antibodies (mAbs). T cells were selected by the positive expression of CD3, whereas B cells were selected from the CD3-negative fraction (Non T cells) and by the positive expression of CD19. CD4-positive and CD8-positive T cells were selected from CD3-positive T cells. Box plots show the percentage of positive cells in each subpopulation for cryo (blue) and cryo+fixed (orange) PBMCs analyzed by flow cytometry. **b** Representative histograms of the mean fluorescent intensity (MFI) with cryopreserved and cryopreserved+fixed PBMCs from healthy donors ($n = 3$) stained with anti-human CD45, CD3, CD19, CD4, and CD8 mAbs. Bar plots show the MFI expression for three fresh and fixed PBMC samples analyzed by flow cytometry. **c**, **d** Representative histograms of MFI of fresh and fixed PBMCs from healthy donors ($n = 4$) stained with anti-human CD45, CD3, CD4, and CD8 mAbs, anti-β2M, anti-CD298, and LMOs analyzed by flow cytometry. **f** Representative histograms of the MFI from cryopreserved (blue) and cryopreserved+fixed (orange) human colon samples processed and stained with anti-human CD45, CD3, CD11b, and EpCAM mAbs and analyzed by flow cytometry. **g** Multiplex fluorescence tissue imaging of a human prostate cancer section, DSP-fixed (*top*) or formalin-fixed (*bottom*) paraffin-embedded, captured using Phenocycler. Images show hematoxylin and eosin staining, five-color overlay, and individual SMA, Pan-CK, E-cadherin, and p63 antibody staining

to formalin-fixed sections, the latter considered to be the "gold standard" (Fig. 7g). This study showcased the potential of DSP fixation in spatial-omics, serving as a proof-of-concept for its application to a broader array of spatial techniques. Additional efforts are underway to extend the use of DSP-fixed tissues to other spatial-omics technologies, such as Visium/Xenium (10x Genomics), GeoMx/CosMx (Nanostring), STereo-seq (BGI), and MERSCOPE (Vizgen).

Discussion

In this study, we introduced the FixNCut protocol, a novel approach that combines sample fixation with subsequent tissue dissociation to overcome several limitations in generating single-cell data. While DSP fixation has previously been used to fix K562 cells and keratinocytes prior to sequencing [16, 17], or in combination with single-cell technologies to explore the adaptive immune repertoire [18], our study is the first to utilize the reversible properties of the DSP fixative with standard enzymatic dissociation on solid biopsies in the context of single-cell transcriptomic studies.

The FixNCut protocol offers significant advantages, including the ability to fix tissue prior to digestion, providing a snapshot of the cell transcriptome at sampling time and minimizing technical artifacts during tissue processing. As the reversible fixative targets proteins rather than nucleic acids, our approach ensures RNA integrity, library complexity, cellular composition, and gene expression comparable to those of the gold-standard fresh RNA sequencing assays. With FixNCut, time and location constraints for sample collection and processing are removed, making it an ideal strategy for research studies involving multiple groups, institutions, and hospitals worldwide.

Standardizing protocols for clinical biopsy collection and downstream processing poses a significant challenge. While single-cell profiling technologies have proven to be highly useful and straightforward for PBMCs and other cells loosely retained in secondary lymphoid tissues, the effective isolation of single cells from solid tissues, such as tumors, remains a technical hurdle. In such cases, single cells may be tightly bound to extracellular scaffolds and neighboring cells, making dissociation and isolation difficult [24]. Additionally, preserving the single-cell transcriptome before scRNA-seq is crucial, particularly when processing multiple samples from biological replicates simultaneously, as it can reduce the need for immediate time-consuming single-cell isolation protocols, such as dissociation, antibody staining, or FACS-based isolation [24]. Recent studies have highlighted the impact of collection and dissociation protocols on cell type proportions and transcriptome profiles in multiple tissue contexts [2–4]. Furthermore, dissociation-related effects have also been observed in cryopreserved human gut mucosa samples [25] and renal biopsies [26]. To overcome these issues, a one-step collagenase protocol was used for intestinal biopsies when no cell type enrichment was required [25]. Meanwhile, the use of cold-active proteases on kidney samples resulted in fewer artifacts, but inefficient tissue dissociation [26]. In addition, studies have shown that neural cell populations (NCPs) suspension without methanol preservation also experiences alterations in cellular composition and gene expression [27]. For fragile tissue biopsies, such as the pancreas or skin, which contain delicate cell populations, cryopreservation and cellular dissociation steps may introduce biases on the cellular composition. We

previously conducted testing of VivoFix [28] with variable results, but acknowledge the potential utility of the protocol for fixation and dissociation.

To address these challenges, we developed FixNCut, an approach that involves reversible fixation of the tissue at the time of collection to prevent further transcriptional changes during downstream processing. This is followed by standard dissociation and storage procedures. At the core of our approach is the use of Lomant's reagent/DSP, a reversible fixative that can easily penetrate cell membranes and preserve tissue characteristics. In this study, we compared fresh and fixed lung and colon samples from different species and experimental scenarios and found comparable results. Additionally, we demonstrated the versatility of the FixNCut for long-term storage by cryopreservation following sample fixation, making it a suitable protocol for its use in more complex and challenging research scenarios. While the lung represents a more resilient tissue for sample processing, without the introduction of major changes in gene expression or cellular composition, colon tissue is very sensitive. Here, we demonstrated decreased RNA quality and a shift in cellular composition in fresh compared to fixed samples, even under standard experimental conditions. We predict that under more stressful conditions, such as therapeutic intervention models, these biases will be even more pronounced.

In single-cell analysis, antibodies are commonly used to select cells of interest by standard FACS enrichment or to quantify cell surface proteins using sequencing (e.g., CITE-Seq). Unlike other fixative agents, such as methanol, which induces protein unfolding and precipitation, or formalin, which non-selectively cross-links proteins, DNA, and RNA (reducing immunoreactivity with target-specific antibodies), the FixNCut protocol has the advantage that cells can be readily stained with antibodies and LMOs. This allows cell labeling or hashing before single-cell analysis. Hence, we assume that this protocol is adaptable and compatible with multiple single-cell modalities, including but not limited to CITE-seq, as well as other droplet or microwell platforms. This versatility makes it a powerful tool for designing flexible and robust studies, being applicable to different tissues, species, or disease conditions.

The FixNCut protocol offers a straightforward way to preserve biopsies for various research contexts, including animal models at research institutes and patient biopsies collected at hospitals. We have demonstrated that FixNCut can be applied in clinical settings, where samples are collected at separate locations and time from their downstream processing steps. The FixNCut protocol shows potential compatibility with multiple single-cell and spatial applications for both single-cell and single-nuclei sequencing, making it a promising versatile tool in various basic, translation, and clinical areas (e.g., oncology and autoimmunity). However, further validation efforts have to reinforce its utility in these diverse applications.

Conclusions

We demonstrate the FixNCut protocol to preserve the transcriptional profile of single cells and the cellular composition of complex tissues. The protocol enables the disconnection of sampling time and location from subsequent processing sites, particularly important in clinical settings. The protocol further prevents sample processing artifacts by stabilizing cellular transcriptomes, enabling robust and flexible study designs for collaborative research and personalized medicine.

Methods

Sample collection

Human PBMC isolation

Peripheral venous blood samples were collected from voluntary blood donors using ACD tubes and stored at 4°C. PBMC isolation was performed using Ficoll density gradient centrifugation. Briefly, 10 mL of blood were diluted with an equal volume of 1× PBS and carefully layered onto 15 mL of Lymphoprep (PN. 15257179, STEMCELL Technologies) followed by centrifugation for 20 min at 800×*g* and room temperature (RT) (with acceleration and brake off). After centrifugation, PBMCs were collected with a sterile Pasteur pipette, transferred to a 15-mL tube, and washed twice with 10 mL of 1× PBS by centrifugation for 5 min at 500×*g* at RT. PBMCs were resuspended in 1× PBS + 0.05% BSA, and cell number and viability were measured with LUNA-FL™ Dual Fluorescence Cell Counter (LogosBiosystem).

Mouse lung collection

C57BL/6 mice were purchased from Janvier Laboratories at 6 weeks of age and sacrificed between weeks 7 and 9 by CO_2 asphyxiation. Lung samples were perfused prior to collection. To perfuse the lungs, a 26-G syringe was used to inject 3 mL of cold Hank's Balanced Salt Solution (HBSS) into the right ventricle of the heart, which resulted in the lungs turning white after injection. Mice were then carefully dissected for further processing.

Mouse colon collection

Mice were sacrificed using as described above, and the colon was collected and washed with HBSS using a syringe to remove feces. The collected colon samples were transported from the facility to the lab in a complete DMEM medium on ice. Upon arrival, the samples were extensively washed with ice-cold PBS and then cut into 3 × 3 mm pieces on a Petri dish using a sterile razor blade. The tissue pieces were then fixed as previously described.

Human colon biopsies

Colonic biopsies were collected from an ulcerative colitis patient in remission and placed in HBSS (Gibco, MA, USA) until processing, which was completed within an hour. The biopsies were split into four different conditions: fresh, fixed, cryopreserved, and fixed/cryopreserved. For fixation, the biopsies were treated as previously described for mouse lung tissue.

Human prostate tissue

Human prostate tissue was collected with informed consent from a 75-year-old patient who underwent a radical prostatectomy procedure for prostate cancer.

Sample preparation: fixation and cryopreservation

Preparation of DSP fixation buffer

A 50× stock solution of DSP (50 mg/mL) was prepared in 100% anhydrous DMSO and stored at −80 °C. Prior to use, 10 µL of the 50× DSP was added dropwise to 490 µL of RT

PBS in a 1.5-mL tube while vortexing to prevent DSP precipitation. This working solution (1× DSP fixation buffer) was then filtered through a 40-µm Flowmi Cell Strainer (PN. BAH136800040-50EA, Sigma-Aldrich). Table 1 provides detailed instructions for using the FixNCut protocol with both the DSP stock solution and working dilution.

PBMCs fixation

One million cells were split into two separate 1.5-mL tubes, with one tube used fresh (as a non-fixed control sample) while the other was subjected to cell fixation. For fixation, cells were centrifuged at 500×*g* for 5 min at 4 °C, and the resulting pellet was resuspended with 500 µL of 1× DSP fixation buffer and incubated at RT. After 15 min, the cells were mixed by pipetting and incubated for an additional 15 min. Fixation was stopped by adding 10 µL of 1 M Tris-HCl pH 7.4, and the sample was briefly vortexed and incubated at RT for 5 min. Both fresh and fixed samples were centrifuged for 5 min at 500×*g* at 4 °C, and contaminating erythrocytes were eliminated by resuspending the pellets and incubating at RT for 5 min with 1× Red Blood Cell lysis solution (PN. 130-094-183, Miltenyi Biotec). Both samples, fresh and fixed, were centrifuged for 5 min at 500×*g* at 4 °C, and contaminating erythrocytes were eliminated by resuspending the pellets in 500 µL of PBS and incubating at RT for 5 min upon addition of 10 times volume of 1× Red Blood Cell lysis solution (PN. 130-094-183, Miltenyi Biotec). Cells were then resuspended in an appropriate volume of 1× PBS + 0.05% BSA in order to reach optimal concentration for cell encapsulation (700–1000 cells/µL) and filtered using a pluriStrainer Mini 40 µm (PN. 43-10040-70 Cell Strainer). Cell concentration was verified with LUNA-FL™ Dual Fluorescence Cell Counter (LogosBiosystem).

Cryopreservation

Cryopreservation of fresh or fixed biopsies was done by transferring them into 1 mL of freezing media (90% FBS + 10% DMSO, Thermo Scientific) and storing them at −80 °C in a Mr. Frosty™ Freezing Container to ensure gradual freezing.

Table 1 Recommendations on working with DSP stock and working dilution, as described by Attar et al. [16]

Preparation of 50× DSP stock
• Equilibrate DSP vial at RT for 30 min and then prepare a 50× stock solution of DSP (50 mg/mL) in anhydrous dimethyl sulfoxide (Sigma, Cat. N. 276855-100ML).
• Dispense the stock into single-use aliquots (e.g., 100 µL aliquots, but volume depends on your use) and store in a bag and dry environment (with silica/desiccant if possible) at −80 °C.
• Be mindful of not opening and closing the tubes at −80 °C.
Preparation of DSP working dilution
• Thaw the 50× DSP stock reagent from −80 °C and equilibrate at RT no longer than 10 min before fixation.
• Immediately before use prepare 500 µL of 1× DSP working solution in molecular biology grade 1× PBS as follows: aliquot 10 µL of 50× DSP stock reagent in a 1.5-mL tube and while vortexing (VERY IMPORTANT) add 490 µL of PBS dropwise using a P200 pipette. 1× DSP must be used within 5 min of preparation.
• *Note: Do not prepare larger volumes (e.g., if you need to fix two samples, prepare each aliquot of 500 µL separately, DO NOT prepare 1 mL and then aliquot into two tubes). You should notice some thin white rings on the walls of the tube once diluted the 50× stock. This is expected and will be cleared during filtration. Stronger precipitation indicates insufficient solving of DSP and preparation of a new dilution is strongly recommended.*
• Filter the 1× DSP working dilution using a 40-µm Flowmi strainer (Sigma, cat. no. BAH136800040-50EA). After filtration 1× DSP can be pooled.
• Do not re-freeze the leftovers of the 50× DSP. Always use a freshly thawed aliquot to prepare the 1× working solution.

Single-cell RNA-seq experimental design (scRNA-seq)

Human PBMC 3′ scRNA-seq

Cells from both fresh and fixed PBMCs were processed for single-cell RNA sequencing using the Chromium Controller system (10X Genomics), with a target recovery of 8000 total cells. The Next GEM Single Cell 3′ Reagent Kits v3.1 (PN-1000268, 10X Genomics) were used to prepare cDNA sequencing libraries, following the manufacturer's instructions. Briefly, after GEM-RT clean-up, cDNA was amplified for 11 cycles and then subjected to quality control and quantification using an Agilent Bioanalyzer High Sensitivity chip (Agilent Technologies). The Dual Index Kit TT Set A (PN-1000215, 10X Genomics) was used for indexing cDNA libraries by PCR. The size distribution and concentration of 3′ cDNA libraries were verified again on an Agilent Bioanalyzer High Sensitivity chip (Agilent Technologies). The cDNA libraries were sequenced on an Illumina NovaSeq 6000 using the following sequencing conditions: 28 bp (Read 1) + 8 bp (i7 index) + 0 bp (i5 index) + 89 bp (Read 2) to generate approximately 40,000 read pairs per cell.

Mouse lung cryopreservation, fixation, and cryopreservation upon fixation

Mouse lungs were harvested and transferred into ice-cold complete DMEM medium. Samples were extensively washed with ice-cold PBS, transferred into a Petri dish, and cut into ~3 × 3 mm pieces using a razor blade. Tissue pieces were divided into four tubes for each condition. Tissue pieces in tube 1 were cryopreserved in freezing media (50% DMEM + 40% FBS + 10% DMSO) and placed into a Mr. Frosty™ Freezing Container and transferred to a −80 °C freezer to ensure a gradual freezing process. The tissue pieces in tubes 2 and 3 were triturated with a razor blade (~1 × 1 mm) on ice and fixed by submerging them in 500 µL of 1X DSP fixation buffer (freshly prepared, within 5 min of use) and incubating at RT for 30 min. After incubation, 10 µL of 1 M Tris-HCl pH 7.5 was added to stop the fixation, and the samples were vortexed for 2–3 s and incubated at RT for 5 min. After a brief centrifugation, the supernatant was removed, and the tissue pieces were washed once with 1 mL of PBS. Tissue pieces in tube 2 were stored at 4 °C in PBS supplemented with 2 U/µL of RNAse inhibitor (Cat. N. 3335402001, Sigma-Aldrich) until the following day, while tissue pieces in tube 3 were cryopreserved by adding 10% DMSO to the PBS, transferring the cell suspension into a cryotube, which was placed into a Mr. Frosty™ Freezing Container, and stored at −80 °C. The tube containing fresh tissue was stored in complete DMEM on ice and washed again with ice-cold PBS before tissue dissociation.

Mouse lung dissociation and scRNA-seq

The day after the collection and storage of samples, the cryopreserved and fixed/cryopreserved samples were quickly thawed in a 37 °C water bath and washed with PBS. Similarly, the fixed sample was washed with PBS before tissue dissociation. The samples were then transferred to a Petri dish on ice and triturated using a razor blade. Next, the small tissue pieces were incubated in 1 mL of digestion media (200 µg/mL Liberase TL, 100 µg/mL DNase I in HBSS with $Ca^{2+}Mg^{2+}$) at 37 °C with shaking at 800 rpm. After 15 min of incubation, the samples were mixed by pipetting, followed by another 15 min of incubation. The cells were then filtered using a pluriStrainer Mini 70 µm (PN. 43-10070-40 Cell Strainer), and the strainer was washed with 10 mL of cold 1X HBSS. The samples

were centrifuged at 500×*g* for 5 min at 4 °C, and the cell pellets were resuspended in 100 µL of PBS + 0.05% BSA. Contaminating erythrocytes were lysed using the previously described method. The cells were washed once with 10 mL PBS + 0.05% BSA, resuspended in an appropriate volume of the same buffer, and filtered using 40-µm strainers. The total number of cells was determined using the LUNA-FL™ Dual Fluorescence Cell Counter (LogosBiosystem). The cell concentration of each sample was adjusted to 700–1000 cells/µL and 7000–10,000 cells were loaded into a 10X Chromium controller. Single-cell RNA-sequencing was performed as described above.

Mouse colon dissociation

Fresh and fixed colon samples were incubated in 1 mL of digestion media (200 U/mL Collagenase IV, 100 µg/mL DNase I in HBSS w/$Ca^{2+}Mg^{2+}$) at 37 °C, shaking at 800 rpm for 30 min. Samples were mixed by pipetting every 10 min during incubation. After the incubation, samples were filtered through a pluriStrainer Mini 70 µm (PN. 43-10070-40 Cell Strainer) and the strainer was washed with 10 mL of cold 1X HBSS. The samples were then centrifuged at 500×*g* for 5 min at 4 °C and cell pellets were washed twice with cold PBS + 0.05% BSA. Finally, the cell pellets were resuspended in an appropriate volume of the same buffer and filtered using 40-µm strainers. The total cell number was determined with the LUNA-FL™ Dual Fluorescence Cell Counter (LogosBiosystem). The cell concentration of each sample was adjusted to 700–1000 cells/µL and 7000 cells were loaded onto a 10X Chromium controller. Single-cell RNA-seq was performed as described above.

Human colon biopsies dissociation

Digestion of biopsies to single-cell suspension was achieved through mechanical and enzymatic digestion as previously described by Veny et al. [29]. Briefly, biopsies were washed in complete medium (CM) (RPMI 1640 medium (Lonza, MD, USA) supplemented with 10% FBS (Biosera, France), 100 U/mL penicillin, 100 U/mL streptomycin and 250 ng/mL amphotericin B (Lonza), 10 µg/mL gentamicin sulfate (Lonza), and 1.5 mM HEPES (Lonza)) before being triturated and incubated in 500 µL of digestion media (CM supplemented with Liberase TM (0.5 Wünsch U/mL) (Roche, Spain) + DNase I (10 µg/mL) (Roche, Spain)) with agitation (250 rpm) for 1 h at 37 °C. After incubation, the cell suspension was filtered using 50-µm and 30-µm cell strainers (CellTrics, Sysmex, USA) to remove cell aggregates and debris. Cell viability and concentration were determined with the LUNA-FL™ Dual Fluorescence Cell Counter (LogosBiosystem). Approximately 7000 cells were loaded onto the Chromium controller (10x Genomics, CA, USA).

Flow cytometric analysis

Flow cytometry analysis of human PBMCs

Anti-human CD3, CD4, CD8, and CD19 antibodies were tested as follows: Cryopreserved PBMCs obtained from three healthy donors were rapidly thawed in a 37 °C water bath. Thawed samples were washed in pre-warmed RPMI media supplemented

with 10% FBS (Thermo Fisher Scientific) and centrifuged at 500×*g* for 5 min at RT. The supernatant was discarded, and pellets were washed in 10 mL of 1× PBS + 0.05% BSA, centrifuged at 500×*g* for 5 min at 4 °C, and resuspended in 1 mL of PBS + 0.05% BSA. The cell suspension was then filtered through a 40-µm cell strainer. Cell viability and concentration were verified using a LUNA-FL™ Dual Fluorescence Cell Counter (LogosBiosystem). Each sample was split into two separate tubes, and half of the cells were fixed with 1× DSP fixation buffer as previously described. After fixation, cells were washed and resuspended in 100 µL of Cell Staining Buffer (PN-420201, Biolegend) and stained with 5 µL of each of the four following primary antibodies: anti-human CD3, CD4, CD8, and CD19 antibody for 15 min at RT in the dark. Detailed information on the antibodies and reagents used in this study is provided in Table 2. Samples were washed twice with Cell Staining Buffer and resuspended in 0.5–1 mL of PBS + 0.05% BSA. 10 µg/mL DAPI (PN-564907, BD Bioscience) was added to determine cell viability before flow cytometric analysis using the BD FACS Melody Automated Cell Sorter (BD Bioscience) and the BD FACSChorus™ Software. Post-acquisition analysis was performed using FlowJo version 10 (FlowJo LLC).

Anti-human CD45, CD3, CD4, and CD8 antibodies and anti-CD298 and β2-microglobulin antibodies were tested as follows: Human PBMCs were isolated from normal donor human buffy coats provided by the Australian Red Cross Blood Service by Ficoll-Paque® density gradient centrifugation. Fresh and fixed PBMCs were incubated with Human BD Fc Block for 10 min at 4°C and then stained for cell surface markers for 30 min at 4 °C according to the manufacturer's recommendation. Annexin V-FITC and PI staining were used to determine viability. Detailed information on the antibodies and reagents used in this study is provided in Table 2. The acquisition was performed on LSR Fortessa X 20 (BD) and analyzed via FlowJo software (FlowJo LLC).

Table 2 Flow cytometry antibodies and reagents

Antibody	Clone	Conjugate	Company
Human BD Fc Block	Fc1	NA	BD # 564219
Anti-human CD45	HI30	BV510	BD # 563204
	HI30	PE	BD Pharmingen
Anti-human CD3	UCHT1	BV711	BD # 563725
	SK7	PE-Cy7	Biolegend PN-344816
	OKT3	PerCP	Biolegend
Anti-human CD4	SK3	BV650	BD # 563875
	RPA-T4	Alexa Fluor® 488	Biolegend PN-300519
Anti-human CD8	HIT8a	PE	BD #555635
	SK1	APC-Cy7	Biolegend PN-344714
Anti-human CD19	6E10	Alexa Fluor® 647	Biolegend PN-302222
Anti-human CD298	LNH-94	PE-Cy7	BioLegend #341707
Anti-human β2-microglobulin	2M2	APC	BioLegend #316311
Anti-human CD11b	ICRF44	PeCy7	Biolegend
Anti-human EPCAM	9C4	APC	Biolegend
Annexin V		FITC	BD #556420
Propidium Iodine			Sigma-Aldrich #P4864

LMO sample preparation

The labeling of PBMCs was performed following the protocol previously described by McGinnis et al. [30]. Briefly, 5 × 105 fresh and fixed PBMCs were washed twice with PBS and labeled with a 1:1 molar ratio of anchor LMO and barcode oligonucleotide for 5 min on ice. Subsequently, both samples were incubated with a co-anchor and Alexa 647 fluorescent oligo feature barcodes at concentrations of 200 nM and 400 nM, respectively, for another 5 min on ice. The cells were then washed twice with ice-cold 1% BSA in PBS. Acquisition was performed on the LSR Fortessa X 20 (BD) and analysis was carried out using FlowJo software (FlowJo LLC). Detailed information on the LMOs used in this study is provided in Table 3.

Flow cytometry analysis of human colon biopsy

The single-cell suspensions obtained after biopsy digestion were labeled with the following antibodies: anti-CD45, anti-CD3, anti-CD11b, and anti-EPCAM, according to the manufacturer's instructions. Detailed information on the antibodies used in this study can be found in Table 2. Cell viability was assessed using the Zombie Aqua Fixable Viability Kit (BioLegend). The cells were then fixed with the Stabilizing Fixative (BD) before being analyzed using the FACSCanto II flow cytometer (BD).

Multiplexing fluorescence tissue imaging

Tissue preparation

The 2 cm × 10 mm tissue sample was divided into two equal halves lengthwise. One half was fixed in 2 ml of 10% neutral buffered formalin (NBF), while the other half was placed in 500 µL of 1X DSP fixation buffer. The NBF-fixed sample was incubated at RT for 4 h, stored overnight at 4 °C, washed 3 times with 1 mL of milliQ water, and then stored in 1 mL of 70% ethanol at 4 °C. The DSP-fixed sample was treated with freshly-made DSP fixation buffer, which was replaced every 60 min for 4 h. The fixed sample was then neutralized with 10 µL of 1M Tris-HCl pH 7.4 for 15 min at RT, washed 3 times with 1 mL of milliQ water, and placed in 1 mL of 70% ethanol at 4°C. Both NBF- and DSP-fixed samples were embedded in paraffin overnight. Five-micrometer-thick sections were cut from both the formalin-fixed, paraffin-embedded (FFPE) and the DSP-fixed paraffin-embedded (DSP-PE) tissues and mounted onto a single poly-L-lysine coated coverslip (22 × 22 mm, #1.5, Akoya Bioscience #7000005).

Table 3 Flow cytometry lipid-modified oligos (LMOs)

Reagent	Sequence	Company
LMO001A Lignoceric Anchor with DNA Oligo	Commercial source	Sigma-Aldrich
LMO001B Palmitic Co-anchor with DNA Oligo	Commercial source	Sigma-Aldrich
A647_Oligos	5'-CCTTGGCACCCGAGAATTCCA-A_647-3 (complementary to the Anchor) or /5Alex647N/CCTTAGCCGCTAATAGGTGAGC (Complementary to Capture sequence of Barcoded Oligo CCTTGGCACCCG AGAATTCCA[Barcode]GCTCACCTATTAGCGGCTAAGG)	Oligo from IDT

Antibody staining

The coverslip mounted section was baked at 60 °C on a heat block for 1 h to remove paraffin, then deparaffinized in 1× Histo-Choice clearing agent (ProSciTech #EMS64110-01) and rehydrated in ethanol before washing in milliQ water. Antigen retrieval was performed in a pressure cooker on the highest setting for 20 min in 1X citrate buffer, pH 6 (Sigma, #C9999-1000ML). The tissue was blocked using buffers from the commercially available Phenocycler staining kit (Akoya Bioscience, # 7000008) and stained with a 7-antibody panel at RT for 3 h. Detailed information on the antibodies used in this study can be found in Table 4. The antibodies were used at a dilution of 0.9:200 for commercially available Akoya antibody-oligo conjugates and 3.7:200 for antibodies custom-conjugated by Akoya Bioscience (Spatial Tissue Exploration Program (STEP)). After staining, the coverslip was subjected to a post-fixation step. DAPI staining was used to visualize cell nuclei and locate regions of interest on each tissue sample with the Zeiss Axio Observer 7 fluorescent inverted microscope.

Phenocycler image acquisition

The Phenocycler microfluidic microscope stage was programmed to acquire two 3 × 3 tiled regions on each tissue using a 20× objective lens, with each tile consisting of a 7-image Z-stack illuminated by LED light to specifically excite either DAPI (for 10 ms in all cycles) or one of three fluorescently labeled reporter oligos (Cy3, Cy5, and Cy7). The software was set to acquire images over 5 cycles, with each cycle consisting of the addition of a set of reporter oligos complementary to the antibody-oligo conjugates detailed in Table 4. During the first and last cycles, no reporter oligos were added to allow for background fluorescence subtraction. The exposure times for each antibody are also provided in Table 4. After imaging was completed, the sample was manually stained with Hematoxylin and Eosin (H&E) following the UofA histology protocol, and bright-field images were captured using the Zeiss Axio Observer 5 fluorescent inverted microscope.

Image processing

The acquired images were processed using the Phenocycler CODEX Processor software (Akoya version 1.8.3.14) to deconvolve and stitch them together, resulting in a set of multi-channel QPTIFF files for each region. The levels for each channel were adjusted using QuPath 0.4.0 and the final images were saved as RGB tiff files. However, some antibodies did not produce sufficient signal or acceptable images after processing and were therefore excluded from further analysis.

Table 4 Antibody and reporter cycle layout, including LED intensities and exposure times for each marker

Cycle #	Cy3 (LED 100%)	Exposure time (ms)	Cy5 (LED 100%)	Exposure time (ms)	Cy7 (LED 60%)	Exposure time (ms)
1	BLANK	250	BLANK	350	BLANK	500
2	e-cadherin-RX014	750	ERG-RX031	850	SMA-RX013	500
3	CD8-RX026	750	CD3e-RX045	850	PanCK-RX019	400
4	Empty	250	p63-RX046	700	Empty	500
5	BLANK	250	BLANK	350	BLANK	500

Data processing

To profile the cellular transcriptome, we processed the sequencing reads using the CellRanger software package (version 6.1.1) from 10X Genomics Inc. We mapped the reads against either the mouse mm10 or the human GRCh38 reference genome (GENCODE v32/Ensembl 98), depending on the samples. In order to avoid any artifacts on the downstream analysis due to differences in sequencing depth among samples, we normalized libraries for effective sequencing depth using "cellranger aggr". This subsampling approach ensures that all libraries have the same average number of filtered reads mapped confidently to the transcriptome per cell.

Data analysis

All analyses presented in this manuscript were conducted using R version 4.0.5, along with specific analysis and data visualization packages. For scRNA-seq analysis, we used the Seurat R package (version 4.0.0) [31], SeuratObject package (version 4.0.1), and other packages specified in the subsequent sections.

scRNA-seq quality control

To compare the library complexity (total captured genes and Unique Molecular Identifiers, or UMIs) across libraries, we investigated the relationship between the cumulative number of detected genes and UMIs with the library sequencing depth. To achieve this, we loaded the "molecule_info.h5" information using the function "read10xMolInfo" from the DropletUtils package (version 1.10.3). Then, we downsampled the library sequenced reads assigned to a barcode (excluding background and noisy reads) using the function "downsample_run", implemented in *Rcpp*, which ensures read sampling without replacement and simultaneously updates the sampling frequency. We utilized various depths for downsampling (steps of 5 M or 10 M reads, depending on the library), which emulates differences in sequencing depth per cell. To assess differences in library complexity along sequencing depth between protocols under study, we fitted a linear regression model ($Y \sim X$) to each curve. Then, we compared the confidence intervals (95% CI) of the independent variable (X, "sequenced reads") across libraries, considering the differences statistically significant when the confidence intervals between conditions did not overlap. Moreover, we assessed the distribution of cell complexity (total captured genes and UMIs) per cell sequencing depth across libraries and computed a linear model to compare the slope of the regression line for each different library. Ultimately, we computed the cumulative number of detected genes over multiple cells by averaging the total genes after 100 sampling of an increasing number of randomly sampled cells (from 1 to 100, using steps of 2), after running the "cellranger aggr" step described above.

To enhance our comprehension of the impact of DSP-fixation on gene recovery, we conducted an analysis comparing the categories of all genes captured in each library—either in all conditions or uniquely in a specific condition of each comparison. For the mouse data, we employed the complete list of gene annotations sourced from the Mouse Genome Informatics website (https://www.informatics.jax.org), while for the human data, we utilized the comprehensive list of gene annotations obtained from the HUGO Gene Nomenclature Committee (HGNC) (https://www.genenames.org/).

After ensuring that there were no remarkable differences in the main quality control (QC) metrics (library size, library complexity, percentage of mitochondrial and ribosomal expression) among the different samples, we performed an independent QC, normalization, and analysis for the libraries from different species and tissue, following the guidelines provided by Luecken et al. [32] and Heumos et al. [33]. We removed low-quality cells by filtering out barcodes with a very low number of UMIs and genes, or with a high percentage of mitochondrial expression, as it is indicative of lysed cells. Additionally, we considered removing barcodes with a large library size and complexity. We eliminated genes that were detected in very few cells. Notably, due to the inherent characteristics of colon biopsies (a higher number of epithelial cells, which are less resistant to sample processing), we followed a slightly different QC approach for mouse and human colon samples. In brief, we performed a first permissive QC filtering out cells with very high MT% (> 75% for mouse and > 85% for human) before proceeding to downstream analysis. We annotated cells to distinguish between the epithelial and non-epithelial fraction. Then, we repeated the QC step, using different thresholds for the epithelial fraction (> 60% MT) and for the non-epithelial cells (> 50% for mouse and > 25% for human). Finally, data was normalized and log-transformed.

Doublet was predicted with Scrublet [34] (version 0.2.3), and computed doublet scores were retained, with putative doublet cell barcodes flagged. However, no threshold was applied to filter them out at this stage, adopting a permissive approach. Consequently, during the clustering and annotation step, the clusters showing modified QC metrics, along with the co-expression of different lineage/population-specific gene markers and high doublet scores, were assessed to determine whether a specific cluster could be classified as a group of doublets and subsequently excluded.

Cell clustering and annotation

To achieve successful cell-type annotation combining data from the same tissue and species (mouse and human colon samples), we removed the batch effect with the *Harmony* integration method [35] using the library as a confounder variable. After integration, we created a k-nearest neighbors (KNN) graph with the "FindNeighbors" function using the first 20 Principal Components (PC), followed by the cell clustering with the Louvain clustering algorithm using the "FindClusters" function at different resolutions. To visualize our data in a two-dimensional embedding, we run the Uniform Manifold Approximation and Projection (UMAP) algorithm. Then, we performed a differential expression analysis (DEA) for all clusters to determine their marker genes using the normalized RNA counts. To annotate the clusters into specific cell types, we examined the expression of canonical gene markers, compared the results of the DE analysis, and referred to gene markers from published annotated datasets. We used the following datasets as references: human PBMCs based on Stuart et al. [36]; mouse lung based on Angelidis et al. [37], Zhang et al. [38], and Bain and MacDonald [39]; mouse colon based on Tsang et al. [40]; and human colon based on Garrido-Trigo et al. [41]. Furthermore, we performed specific cell-type sub-clustering when required a fine-grained resolution to capture a specific cell state of interest. Doublets and low-quality cells were automatically removed at this point.

Comparison of gene expression profiles

Gene expression correlation analysis

The overall similarity of pseudo-bulk gene expression profiles across experimental conditions was explored using the Pearson correlation (r^2). To generate the pseudo-bulk profiles, we computed the mean of the log-average gene counts across all cells per sample, as well as for each defined cell population independently. Due to the sparsity of scRNA-seq data, we only computed correlation for the cell types with over 100 cells and only if over 20 cells were present by condition to compare. Additionally, to avoid biases driven by cell populations with different sizes, we randomly downsampled the number of cells to the condition having fewer cells. To assess the strength and significance of the correlation, we used linear regression models; we considered a strong significant linear correlation when $r^2 > 0.9$ and p-value < 0.05.

Compositional analysis

To estimate the changes in the proportions of cell populations across experimental conditions, we applied the *scCODA* package (version 0.1.2) [42], a Bayesian approach that considers inherent biases in cell-type compositions and addresses the low-replicate issue, making it an appropriate tool for our experimental design. This compositional analysis depends on a reference cell type, and credible changes (nominal FDR < 0.05) for varying log-fold changes should be interpreted in relation to the selected reference cell type. For this reason, we used the "automatic" selection of reference cell type for single comparisons, but we set a manual "pre-selected reference" cell type when multiple comparisons were conducted against the same condition. In the latter case, we tested multiple reference cells to ensure consistent results.

Differential expression analysis (DEA)

To define condition-specific signatures, we performed differential expression analysis (DEA) using the Seurat function "*FindMarkers*" with the MAST test. We defined genes to be significantly differentially expressed (sDE) if the Log2 Fold Change (Log2FC) > |1|, with a false discovery rate (FDR) adjusted p-value < 0.05, and if they were present in at least 10% of cells.

Gene Set Enrichment Analysis (GSEA)

To unravel biological pathways affected by a specific condition, we performed a pre-ranked GSEA with the *fgsea* package [43] and employed multiple gene sets from the Human Molecular Signatures Database (MSigDB), specifically, the mouse and human Hallmarks (H), Canonical Curated Pathways (C2:CP) such as Reactome, and Gene Ontology (C5:GO) gene sets from Biological Process (BP). We excluded gene sets that did not satisfy our pathway size criteria (10–300 genes) and considered significant only results with an FDR adjusted p-value < 0.05, where > 5 genes overlapped with the gene set, and this accounted for > 15% of the gene set.

Condition-specific signatures

To evaluate the effectiveness of the FixNCut protocol in preventing cells from undergoing stress, we assessed condition-specific signatures and sDE genes associated with external stressors. For human PBMC samples, we included publicly available signatures, such as the ex vivo PBMC handling signature on microarrays by Baechler et al. [44] and the human PBMC sampling time-dependent signature on single-cell by Massoni-Badosa et al. [4]. Additionally, we studied multiple dissociation-induced gene expression signatures for the tissue samples, including dissociation on mouse muscle stem cells by van den Brink et al. [22], warm-dissociation on mouse kidney samples by Denisenko et al. [3], and warm collagenase on mouse primary tumors and patient-derived mouse xenografts by O'Flanagan et al. [2]. With this purpose, we downloaded the sDE genes from these studies and computed signature-specific scores using the *Ucell* package [45]. To account for biases arising from differences in cell population numbers across protocols, we downsampled at a maximum of 250 cells per cell type. Moreover, we also investigated the expression of specific genes across cell populations and conditions. Statistical analysis between sample protocols was performed using the Wilcoxon signed-rank test.

Abbreviations

ACME	ACetic-MEthanol
CM	Complete Media
DEA	Differential expression analysis
DSP	Dithiobis(succinimidyl propionate)
DSP-PE	DSP-fixed, paraffin-embedded
FFPE	Formalin-fixed, paraffin-embedded
GEM	Gel Beads-in-emulsion
GSEA	Gene Set Enrichment Analysis
H&E	Hematoxylin and eosin
HBSS	Hank's Balanced Salt Solution
HVG	Highly variable gene
IBD	Inflammatory bowel disease
LMO	Lipid-modified oligo
mAbs	Monoclonal antibodies
ME	Mean expression
MFI	Mean fluorescent intensity
NCP	Neural cell populations
NHS ester	N-Hydroxysuccinimide ester
PBMC	Peripheral blood mononuclear cell
PC	Principal components
QC	Quality control
ROS	Reactive oxygen species
RT	Room temperature
STEP	Spatial Tissue Exploration Program
UMAP	Uniform manifold approximation and projection
UMI	Unique molecular identifier
UPR	Unfolded protein response

Supplementary Information

The online version contains supplementary material available at https://doi.org/10.1186/s13059-024-03219-5.

Additional file 1: Supplementary Figures. *Supplementary Figures 1-6 and Supplementary figure legends.*

Additional file 2: Table 1. This table contains the differentially expressed (DE) genes between fixed and fresh human peripheral blood mononuclear cells (PBMCs), considering all cell populations. The differential expression analysis was performed using Seurat MAST, and genes with an FDR adjusted p-value < 0.05 and present in at least 10% of cells were considered DE (see Methods). Genes with positive Log2FC indicate higher expression in fixed PBMCs, while those with negative Log2FC are DE in fresh PBMCs.

Additional file 3: Table 2. This table contains differentially expressed (DE) genes between fixed and fresh human PBMCs, separated by cell population. The analysis was performed using Seurat MAST, with genes considered as DE with a FDR adjusted p-value < 0.05 and present in at least 10% of cells (see Methods). A positive Log2FC value indicates higher expression in fixed PBMCs, while a negative value indicates differential expression in fresh PBMCs.

Additional file 4: Table 3. This table contains differentially expressed (DE) genes for mouse tissue comparisons, considering all cell populations. The comparisons include: 1) fixed versus fresh lung samples, 2) fixed versus fresh colon samples, 3) fixed compared to cryopreserved (cryo), 4) fixed/cryo versus cryo, and 5) fixed/cryo compared with fixed on lung samples. The statistical analysis was performed using Seurat MAST with genes considered DE if they had an FDR adjusted p-value < 0.05 and were present in at least 10% of cells (see Methods). The results include positive Log2FC values indicating higher expression in the first condition mentioned, while negative values indicate higher expression in the second condition mentioned.

Additional file 5: Table 4. This table contains the list of differentially expressed (DE) genes between fixed and fresh mouse lung samples, categorized by cell population. The test was performed using Seurat MAST, where genes with a FDR adjusted p-value < 0.05 and present in at least 10% of cells were considered as DE (see Methods). The Log2FC values indicate the direction of expression change, where positive values indicate higher expression in fixed samples and negative values indicate higher expression in fresh samples.

Additional file 6: Table 5. This table contains the results of gene set enrichment analysis (GSEA) between fixed and fresh mouse lung samples by cell population. The analysis was performed using the *fgsea* package and multiple gene sets from MSigDB. Gene sets containing 10-300 genes were included, and only results with a FDR adjusted p-value < 0.05 were considered if they contained >5 overlapping genes, which represents >15% of the gene set (see Methods).

Additional file 7: Table 6. This table contains the differentially expressed (DE) genes between fixed and fresh mouse colon samples, analyzed by cell population using Seurat MAST. Genes were considered DE if they had an FDR adjusted p-value < 0.05 and were present in at least 10% of cells (see Methods). The Log2FC value indicates whether the gene is more highly expressed in fixed (positive values) or fresh (negative values) samples.

Additional file 8: Table 7. This table contains the results of gene set enrichment analysis (GSEA) between fixed and fresh mouse colon samples by cell population. The analysis was performed using the *fgsea* package and multiple gene sets from MSigDB. Gene sets containing 10-300 genes were included, and results were considered significant if they had an FDR adjusted p-value < 0.05 and if >5 genes from the gene set overlapped with the differentially expressed genes, representing more than 15% of the gene set (see Methods).

Additional file 9: Table 8. This table contains differentially expressed (DE) genes between fixed/cryo and cryo mouse lung samples, analyzed by cell population. The test was performed with Seurat MAST, and genes were considered DE with a FDR adjusted p-value < 0.05, and present in at least 10% of cells (see Methods). A positive Log2FC indicates higher expression in fixed or fixed/cryo samples, whereas negative values indicate differential expression in cryo or fixed samples.

Additional file 10: Table 9. This table contains the results of gene set enrichment analysis (GSEA) for fixed/cryo versus cryo mouse lung samples, by cell population. The analysis was performed using the *fgsea* package with multiple gene sets from MSigDB. Gene sets containing within 10-300 genes were included and the obtained results were considered significant if the FDR adjusted p-value was <0.05 and if >5 genes overlapped with the gene set, representing >15% of the gene set (see Methods).

Additional file 11: Table 10. This table contains differentially expressed (DE) genes for human colon biopsies comparisons, considering all cell populations. The comparisons include: 1) fixed and fresh, 2) fixed and cryo, 3) fixed/cryo versus cryo, and 4) fixed/cryo compared with fixed samples. The analysis was performed using Seurat MAST, and genes were considered DE with a FDR adjusted p-value < 0.05 and present in at least 10% of cells (see Methods). A positive Log2FC indicates higher expression in fixed or fixed/cryo samples, whereas negative values indicate differential expression in fresh, cryo or fixed samples.

Additional file 12: Table 11. This table contains the differentially expressed (DE) genes between fixed and fresh human colon biopsies, separated by cell population. The test was performed using Seurat MAST, with genes considered DE if they had a FDR adjusted p-value < 0.05 and were present in at least 10% of cells (see Methods). Positive Log2FC values indicate higher expression in fixed samples, while negative values indicate higher expression in fresh samples.

Additional file 13: Table 12. This table contains the differentially expressed (DE) genes between fixed/cryo versus cryo human colon biopsies, separated by cell population. The test was performed using Seurat MAST, with genes considered DE if they had a FDR adjusted p-value < 0.05 and were present in at least 10% of cells (see Methods). Positive Log2FC values indicate higher expression in fixed/cryo samples, while negative values indicate higher expression in cryo samples.

Additional file 14: Table 13. This table contains the results of gene set enrichment analysis (GSEA) for fixed versus fresh human colon biopsies comparison by cell population. The test was performed with the *fgsea* package using multiple gene sets from MSigDB. Gene sets were included only if they contained between 10-300 genes, and obtained results were considered with a FDR adjusted p-value < 0.05, only if more than 5 genes were overlapping with the gene set and represented more than 15% of the gene set (see Methods).

Additional file 15: Table 14. This table contains the results of gene set enrichment analysis (GSEA) for fixed/cryo versus cryo h uman colon biopsies comparison by cell population. The test was performed with the *fgsea* package using multiple gene sets from MSigDB. Gene sets were included only if they contained between 10-300 genes, and obtained results were considered with a FDR adjusted p-value < 0.05, only if more than 5 genes were overlapping with the gene set and represented more than 15% of the gene set (see Methods).

Additional file 16. Peer review history.

Acknowledgements
The LMO oligos used were kindly provided by Chris McGinnis from the Gartner lab (UCSF). The authors would like to thank the CRG Scientific IT Unit and the maintainers of the CNAG-CRG compute cluster for providing assistance with essential computing resources. Also, the authors would like to thank all the team members for their contributions during brainstorming and discussion sessions.

Review history
The review history is available as Additional file 16.

Disclaimer
Content of this publication reflects only the author's view and the JU is not responsible for any use that may be made of the information it contains.

Peer review information
Tim Sands was the primary editor of this article and managed its editorial process and peer review in collaboration with the rest of the editorial team.

Authors' contributions
H.H. and L.G.M. designed the study. L.G.M. and J.P. devised the use of DSP for fixing tissues following dissociation. D.M. and G.C. performed the scRNA-seq experiments. L.J.-G. and J.C.N. annotated all datasets. L.J.-G. performed the computational analysis. D.M., J.C.N., S.R., E.M.-A., and V.G. performed and analyzed the FACS data. K.W. and K.B.J. performed the CODEX experiments. H.-M. performed all mice work. N.K.R., L.M.B., J.P.B., F.T., L.K.S., S.S., M.v.d.B., T.K, P.L.v.d.V., M.C.N., P.R., and A.S. provided clinical material. L.J.-G., D.M., and J.C.N. prepared the figures. L.J.-G, D.M, H.H., and L.G.M. wrote the manuscript with contributions from all the co-authors. All authors read and approved the current version of the manuscript.

Funding
This project has received funding from the Innovative Medicines Initiative 2 Joint Undertaking (IMI 2 JU) under grant agreement No 831434 (3TR; Taxonomy, Targets, Treatment, and Remission). The JU receives support from the European Union's Horizon 2020 research and innovation program and EFPIA. Also, this project has received funding from the European Union's H2020 research and innovation program under grant agreement No 848028 (DoCTIS; Decision On Optimal Combinatorial Therapies In Imids Using Systems Approaches). L.J.-G. has held an FPU PhD fellowship (FPU19/04886) from the Spanish Ministry of Universities. V.G. is supported by grant #2008-04050 from The Leona M. and Harry B. Helmsley Charitable Trust. E.M. is funded by grant RH042155 (RTI2018-096946-B-I00) from Ministerio de Ciencia e Innovacion. I.A.P holds a Victorian Cancer Agency Mid-Career Fellowship 2019. A.S. is funded by PID2021-123918OB-I00 from MCIN/AEI/51 10.13039/501100011033 and co-funded by "FEDER: A way to make Europe". Australian Prostate Cancer BioResource (APCB) collection in Adelaide is supported by funding from the South Australian Immunogenomics Cancer Institute and the South Australian Health and Medical Research Institute.

Availability of data and materials
The complete raw data (FASTQ files) and count matrices generated in this study have been submitted to the NCBI Gene Expression Omnibus (GEO) under accession number GSE229944 (https://www.ncbi.nlm.nih.gov/geo/query/acc.cgi?acc=GSE229944) [46]. The processed scRNA-seq datasets and metadata (R objects, Seurat) analyzed in the current study have been deposited at Zenodo (https://doi.org/10.5281/zenodo.10468192) [47].
The detailed DSP-fixation protocol can be accessed at Protocols.io (https://www.protocols.io/view/fixncut-v1-0-14egn3xjql5d/v1) [48].
The code to reproduce the full analysis is hosted at GitHub https://github.com/LJimenezGracia/FIXnCUT_benchmarking [49].

Declarations

Ethics approval and consent to participate
Experiments with mice were conducted in accordance with the guidelines of the Animal Care and Use Committee of Barcelona Science Park (protocol CEEA-PCB-14-000275). Healthy PBMC donors were collected with written informed consent at the Centro Nacional de Análisis Genómico (CNAG). Healthy human buffy coats were provided by the Australian Red Cross Blood Service, and the ethical approval was obtained by the Melbourne Human Ethics Committee (01/14). Colon biopsies from Ulcerative Colitis patients in remission were collected with written informed consent at the Hospital Clinic of Barcelona with ethical approval granted by the clinical research ethics committee of the Hospital Clínic of Barcelona (Reg. HCB/2022/0125). Prostate tissues were collected with written informed consent from previously untreated patients undergoing radical prostatectomy at St. Andrew's Hospital, Adelaide, Australia, through the Australian Prostate Cancer BioResource. Ethical approval for tissue collection and experimentation was obtained from St Andrew's (#80) and the University of Adelaide (H-2012-016) Human Research Ethics committees. This study was conducted in accordance with the Declaration of Helsinki principles.

Consent for publication
Not applicable.

Competing interests
H.H. is a co-founder and shareholder of Omniscope, a scientific advisory board member of MiRXES and Nanostring, and a consultant to Moderna and Singularity. L.G.M is an advisor and shareholder of Omniscope and advisor for ArgenTAG, Millenium Sciences, and Truckee Applied Genomics. J.C.N. is a consultant of Omniscope. M.C.N. has received grants (unrestricted) from GSK, the European Commission, and Lung Foundation Netherlands. M.v.d.B. has received grants (unrestricted) from AstraZeneca, Novartis, GlaxoSmithKline, Roche, Genentech, and Sanofi. F.T. received speaker's fees from Falk, Janssen, and AbbVie. S.S. has been a consultant for AbbVie, Bristol Myers Squibb, Boehringer Ingelheim, Ferring, Genentech/Roche, Janssen, Lilly, Novartis, Merck Sharp Dohme, Medimmune/AstraZeneca, Pfizer, Protagonist, Sanofi, Takeda, Theravance, and UCB and is a paid speaker for AbbVie, Ferring, Janssen, Merck Sharp Dohme, Novartis, Takeda, and UCB. P.R. has been a consultant for Takeda and Omass. I.A.P. holds current research grants with AstraZeneca and BMS. Omniscope has filed a patent related to the application of the FixNCut protocol. All other authors declare no competing interests.

Author details
[1]Centro Nacional de Análisis Genómico (CNAG), 08028 Barcelona, Spain. [2]Universitat de Barcelona (UB), Barcelona, Spain. [3]Inflammatory Bowel Disease Group, Institut d'Investigacions Biomèdiques August Pi i Sunyer (IDIBAPS), Barcelona, Spain. [4]Centro de Investigación Biomédica en Red de Enfermedades Hepáticas y Digestivas (CIBEREHD), Barcelona, Spain. [5]Cancer Immunology Program, Peter MacCallum Cancer Centre, Melbourne, VIC, Australia. [6]Sir Peter MacCallum Department of Oncology, The University of Melbourne, Melbourne, VIC, Australia. [7]Monash University Department of Surgery, Alfred Hospital, Melbourne, VIC, Australia. [8]Adelaide Centre for Epigenetics (ACE), University of Adelaide, Adelaide, South Australia, Australia. [9]South Australian immunoGENomics Cancer Institute (SAiGENCI), University of Adelaide, Adelaide, South Australia, Australia. [10]Australian Genomics Research Facility, Adelaide, South Australia, Australia. [11]Freemasons Foundation Centre for Men's Health, University of Adelaide, Adelaide, South Australia, Australia. [12]South Australian Health and Medical Research Institute, Adelaide, South Australia, Australia. [13]Institute for Research in Biomedicine (IRB Barcelona), The Barcelona Institute of Science and Technology, Barcelona, Spain. [14]Centro de Investigación Biomédica en Red de Cáncer (CIBERONC), Barcelona, Spain. [15]Institute of Clinical Molecular Biology, Kiel University, Kiel, Germany. [16]Department of Internal Medicine I, University Hospital Schleswig-Holstein (UKSH), Campus Kiel, Kiel, Germany. [17]Department of Pulmonary Diseases, University of Groningen, University Medical Center Groningen, Groningen, Netherlands. [18]Groningen Research Institute for Asthma and COPD, University of Groningen, University Medical Center Groningen, Groningen, Netherlands. [19]Department of Pathology & Medical Biology, University of Groningen, University Medical Center Groningen, Groningen, Netherlands. [20]ICREA, Barcelona, Spain. [21]St Jude Children's Research Hospital, Memphis, TN 38105, USA. [22]Omniscope, Barcelona, Spain.

Received: 12 April 2023 Accepted: 18 March 2024
Published online: 29 March 2024

References

1. Ziegenhain C, Vieth B, Parekh S, Hellmann I, Enard W. Quantitative single-cell transcriptomics. Brief Funct Genomics. 2018;17:220–32.
2. O'Flanagan CH, Campbell KR, Zhang AW, Kabeer F, Lim JLP, Biele J, et al. Dissociation of solid tumor tissues with cold active protease for single-cell RNA-seq minimizes conserved collagenase-associated stress responses. Genome Biol. 2019;20:210.
3. Denisenko E, Guo BB, Jones M, Hou R, de Kock L, Lassmann T, et al. Systematic assessment of tissue dissociation and storage biases in single-cell and single-nucleus RNA-seq workflows. Genome Biol. 2020;21:130.
4. Massoni-Badosa R, Iacono G, Moutinho C, Kulis M, Palau N, Marchese D, et al. Sampling time-dependent artifacts in single-cell genomics studies. Genome Biol. 2020;21:112.
5. Marsh SE, Walker AJ, Kamath T, Dissing-Olesen L, Hammond TR, de Soysa TY, et al. Dissection of artifactual and confounding glial signatures by single-cell sequencing of mouse and human brain. Nat Neurosci. 2022;25:306–16.
6. Boonlayangoor P, Telischi M, Boonlayangoor S, Sinclair TF, Millhouse EW. Cryopreservation of human granulocytes: study of granulocyte function and ultrastructure. Blood. 1980;56:237–45.
7. Kotsakis A, Harasymczuk M, Schilling B, Georgoulias V, Argiris A, Whiteside TL. Myeloid-derived suppressor cell measurements in fresh and cryopreserved blood samples. J Immunol Methods. 2012;381:14–22.
8. de Ruiter K, van Staveren S, Hilvering B, Knol E, Vrisekoop N, Koenderman L, et al. A field-applicable method for flow cytometric analysis of granulocyte activation: cryopreservation of fixed granulocytes. Cytom Part J Int Soc Anal Cytol. 2018;93:540–7.
9. Wang X, Yu L, Wu AR. The effect of methanol fixation on single-cell RNA sequencing data. BMC Genomics. 2021;22:420.
10. García-Castro H, Kenny NJ, Iglesias M, Álvarez-Campos P, Mason V, Elek A, et al. ACME dissociation: a versatile cell fixation-dissociation method for single-cell transcriptomics. Genome Biol. 2021;22:89.
11. Katzenelenbogen Y, Sheban F, Yalin A, Yofe I, Svetlichnyy D, Jaitin DA, et al. Coupled scRNA-Seq and intracellular protein activity reveal an immunosuppressive role of TREM2 in cancer. Cell. 2020;182:872-885.e19.
12. Phan HV, van Gent M, Drayman N, Basu A, Gack MU, Tay S. High-throughput RNA sequencing of paraformaldehyde-fixed single cells. Nat Commun. 2021;12:5636.
13. Vértesy Á, Eichmueller OL, Naas J, Novatchkova M, Esk C, Balmaña M, et al. Cellular stress in brain organoids is limited to a distinct and bioinformatically removable subpopulation. bioRxiv. 2022:2022.03.11.483643. https://doi.org/10.1101/2022.03.11.483643v1.

14. Machado L, Relaix F, Mourikis P. Stress relief: emerging methods to mitigate dissociation-induced artefacts. Trends Cell Biol. 2021;31:888–97.
15. Machado L, Geara P, Camps J, Santos MD, Teixeira-Clerc F, Herck JV, et al. Tissue damage induces a conserved stress response that initiates quiescent muscle stem cell activation. Cell Stem Cell. 2021;28:1125-1135.e7.
16. Attar M, Sharma E, Li S, Bryer C, Cubitt L, Broxholme J, et al. A practical solution for preserving single cells for RNA sequencing. Sci Rep. 2018;8:2151.
17. Gerlach JP, van Buggenum JAG, Tanis SEJ, Hogeweg M, Heuts BMH, Muraro MJ, et al. Combined quantification of intracellular (phospho-)proteins and transcriptomics from fixed single cells. Sci Rep. 2019;9:1469.
18. Nesterenko PA, McLaughlin J, Cheng D, Bangayan NJ, Burton Sojo G, Seet CS, et al. Droplet-based mRNA sequencing of fixed and permeabilized cells by CLInt-seq allows for antigen-specific TCR cloning. Proc Natl Acad Sci. 2021;118:e2021190118.
19. Baechler EC, Batliwalla FM, Karypis G, Gaffney PM, Moser K, Ortmann WA, et al. Expression levels for many genes in human peripheral blood cells are highly sensitive to ex vivo incubation. Genes Immun. 2004;5:347–53.
20. Arceneaux D, Chen Z, Simmons AJ, Heiser CN, Southard-Smith AN, Brenan MJ, et al. A contamination focused approach for optimizing the single-cell RNA-seq experiment. iScience. 2023;26:107242.
21. Habib N, Li Y, Heidenreich M, Swiech L, Avraham-Davidi I, Trombetta JJ, et al. Div-Seq: Single-nucleus RNA-Seq reveals dynamics of rare adult newborn neurons. Science. 2016;353:925–8.
22. van den Brink SC, Sage F, Vértesy Á, Spanjaard B, Peterson-Maduro J, Baron CS, et al. Single-cell sequencing reveals dissociation-induced gene expression in tissue subpopulations. Nat Methods. 2017;14:935–6.
23. Black S, Phillips D, Hickey JW, Kennedy-Darling J, Venkataraaman VG, Samusik N, et al. CODEX multiplexed tissue imaging with DNA-conjugated antibodies. Nat Protoc. 2021;16:3802–35.
24. Haque A, Engel J, Teichmann SA, Lönnberg T. A practical guide to single-cell RNA-sequencing for biomedical research and clinical applications. Genome Med. 2017;9:75.
25. Uniken Venema WTC, Ramírez-Sánchez AD, Bigaeva E, Withoff S, Jonkers I, McIntyre RE, et al. Gut mucosa dissociation protocols influence cell type proportions and single-cell gene expression levels. Sci Rep. 2022;12:9897.
26. Deleersnijder D, Callemeyn J, Arijs I, Naesens M, Van Craenenbroeck AH, Lambrechts D, et al. Current methodological challenges of single-cell and single-nucleus RNA-sequencing in glomerular diseases. J Am Soc Nephrol JASN. 2021;32:1838–52.
27. Gutiérrez-Franco A, Hassan MN, Mularoni L, Plass M. Methanol fixation is the method of choice for droplet-based single-cell transcriptomics of neural cells. bioRxiv. 2022:2022.08.03.502652. https://doi.org/10.1101/2022.08.03.502652v1.
28. Fortmann SD, Frey BF, Hanumanthu VS, Liu S, Goldsborough A, Kilchrist KV, et al. Fixation before dissociation using a deep eutectic solvent preserves in vivo states and phospho-signaling in single-cell sequencing. bioRxiv. 2023:2023.02.13.528370. https://doi.org/10.1101/2023.02.13.528370v1.
29. Veny M, Garrido-Trigo A, Corraliza AM, Masamunt MC, Bassolas-Molina H, Esteller M, et al. Dissecting common and unique effects of anti-α4β7 and anti-tumor necrosis factor treatment in ulcerative colitis. J Crohns Colitis. 2021;15:441–52.
30. McGinnis CS, Patterson DM, Winkler J, Conrad DN, Hein MY, Srivastava V, et al. MULTI-seq: sample multiplexing for single-cell RNA sequencing using lipid-tagged indices. Nat Methods. 2019;16:619–26.
31. Hao Y, Hao S, Andersen-Nissen E, Mauck WM, Zheng S, Butler A, et al. Integrated analysis of multimodal single-cell data. Cell. 2021;184:3573-3587.e29.
32. Current best practices in single-cell RNA-seq analysis: a tutorial. Molecular Systems Biology. 2023. https://doi.org/10.15252/msb.20188746.
33. Heumos L, Schaar AC, Lance C, Litinetskaya A, Drost F, Zappia L, et al. Best practices for single-cell analysis across modalities. Nat Rev Genet. 2023;24:550–72.
34. Wolock SL, Lopez R, Klein AM. Scrublet: computational identification of cell doublets in single-cell transcriptomic data. Cell Syst. 2019;8:281-291.e9.
35. Korsunsky I, Millard N, Fan J, Slowikowski K, Zhang F, Wei K, et al. Fast, sensitive and accurate integration of single-cell data with Harmony. Nat Methods. 2019;16:1289–96.
36. Stuart T, Butler A, Hoffman P, Hafemeister C, Papalexi E, Mauck WM, et al. Comprehensive Integration of Single-Cell Data. Cell. 2019;177:1888-1902.e21.
37. Angelidis I, Simon LM, Fernandez IE, Strunz M, Mayr CH, Greiffo FR, et al. An atlas of the aging lung mapped by single cell transcriptomics and deep tissue proteomics. Nat Commun. 2019;10:963.
38. Zhang H, Kang Z, Gong H, Xu D, Wang J, Li Z, et al. Digestive system is a potential route of COVID-19: an analysis of single-cell coexpression pattern of key proteins in viral entry process. Gut. 2020;69:1010–8.
39. Bain CC, MacDonald AS. The impact of the lung environment on macrophage development, activation and function: diversity in the face of adversity. Mucosal Immunol. 2022;15:223–34.
40. Tsang DKL, Wang RJ, De Sa O, Ayyaz A, Foerster EG, Bayer G, et al. A single cell survey of the microbial impacts on the mouse small intestinal epithelium. Gut Microbes. 2022;14:2108281.
41. Garrido-Trigo A, Corraliza AM, Veny M, Dotti I, Melon-Ardanaz E, Rill A, et al. Macrophage and neutrophil heterogeneity at single-cell spatial resolution in inflammatory bowel disease. bioRxiv. 2022:2022.11.28.518139. https://doi.org/10.1101/2022.11.28.518139v1.
42. Büttner M, Ostner J, Müller CL, Theis FJ, Schubert B. scCODA is a Bayesian model for compositional single-cell data analysis. Nat Commun. 2021;12:6876.
43. Korotkevich G, Sukhov V, Budin N, Shpak B, Artyomov MN, Sergushichev A. Fast gene set enrichment analysis. bioRxiv. 2021:060012. https://doi.org/10.1101/060012v3.
44. Expression levels for many genes in human peripheral blood cells are highly sensitive to ex vivo incubation | Genes & Immunity [Internet]. [cited 2023 Mar 23]. Available from: https://www.nature.com/articles/6364098.
45. Andreatta M, Carmona SJ. UCell: Robust and scalable single-cell gene signature scoring. Comput Struct Biotechnol J. 2021;19:3796–8.

46. Jiménez-Gracia L, Heyn H, Martelotto L. FixNCut: Single-cell genomics through reversible tissue fixation and dissociation. GSE229944. Gene Expression Omnibus. 2024. https://www.ncbi.nlm.nih.gov/geo/query/acc.cgi?acc=GSE229944.
47. Jiménez-Gracia L, Heyn H, Martelotto L. FixNCut: Single-cell genomics through reversible tissue fixation and dissociation. Zenodo. 2024. https://doi.org/10.5281/zenodo.10468192.
48. Jiménez-Gracia L, Heyn H, Martelotto L. FixNCut v1.0. Protocols.io. 2023. https://doi.org/10.17504/protocols.io.14egn3xjql5d/v1.
49. Jiménez-Gracia L, Heyn H, Martelotto L. FIXnCUT_benchmarking. GitHub; 2023. https://github.com/LJimenezGracia/FIXnCUT_benchmarking .

Publisher's Note